UTILIZATION OF TEMPERATURE DATA TO DETERMINE RESERVOIR THICKNESS

A THESIS
SUBMITTED TO THE DEPARTMENT OF
ENERGY RESOURCES ENGINEERING
OF STANFORD UNIVERSITY
IN PARTIAL FULFILLMENT OF THE REQUIREMENTS
FOR THE DEGREE OF
MASTER OF SCIENCE

Ha-andza Mabunda

June 2014

I certify that I have read this thesis and that in my opinion it is fully adequate, in scope and quality, as partial fulfillment of the degree of Master of Science in Petroleum Engineering.

(Roland Horne) Principal Adviser

Abstract

Knowledge of reservoir thickness is crucial in the determination of the hydrocarbon volumes in a reservoir. An incorrect estimation of reservoir thickness, therefore, would lead to an incorrect reserves estimation. During traditional pressure transients analysis, reservoir thickness is often assumed constant to enable the determination of reservoir permeability. Permeability estimates from pressure transient analysis have been used as decision anchors for performance of reservoir stimulations. In this sense, by the assumption of constant-reservoir thickness, decisions made on such permeability calculations are based on misleading data. Here, we investigate the utility of temperature as a matching parameter to determine reservoir thickness. We used the Levenberg-Marquardt algorithm to determine the reservoir thickness which would minimize the difference between reservoir temperature and model temperature. Eclipse 300 was used to generate temperature profiles. Using temperature data, reservoir thickness could be determined in a partially penetrated reservoir. In other reservoir shapes, information on the nonuniformity of the reservoir could be extracted from the mismatch of the reservoir temperature data with a temperature profile using a model assumed to have constant reservoir thickness.

Acknowledgements

I would like to extend my gratitude towards the SUPRI-D research group for allowing me the opportunity to work on this problem through its financial generosity. I would like to thank my dear friends (Marcia Baloyi, Tsakani Malwandla, Amu Mhangwani/Maluleke, Nsovo Mathetheswa and Mpho Makhubele) who managed to put at the least a smile on my face from 10,000 miles away. Weekday mornings would not have been the same without you guys. Craig Dube, for everything since our Tech days. A big thank you goes to my mother who I don't tell enough how much I love. And to my sister. Hoyozelani Mabunda, I hope that one day you will find inspiration in the things that I do.

And last but not least, thank you to Roland Horne, my wonderful adviser. Your patience with me has amazed me every week. I know I would not have been able to do any of this without you. I am forever grateful.

Contents

Abstract **iii**

Acknowledgements **iv**

1 Introduction and Problem Statement **1**

2 Literature Review **3**

3 Methodology **6**

3.1 Grid Construction 6

3.2 Fluid and Rock Properties 10

3.3 Well placement and Timestep 11

3.4 Thickness Estimation Procedure 13

3.5 Summary 16

4 Sensitivity Analysis **18**

4.1 Sensitivity to Porosity 19

4.2 Sensitivity to Formation Heat Conductivity 22

4.3 Sensitivity to Oil Density 25

4.4 Sensitivity to Specific Heat 28

4.5 Sensitivity to Thermal Expansion Coefficient 31
4.6 Sensitivity to Oil Viscosity 34
4.7 Sensitivity to Geothermal Gradient 37
4.7.1 Changing Temperature for Gradient-Calculation Models with Constant Permeability-Thickness Product 39
4.7.2 Gradient-Calculation Models with Temperature Similar to Thickness-Prediction Model Temperature and Constant Permeability-Thickness Product 42
4.7.3 Gradient-Calculation Models with Temperature Similar to Thickness-Prediction Model Temperature and Constant Permeability . . 45
4.8 Summary 47

5 Results and Discussion 49

5.1 Homogeneous Reservoir with Constant Thickness and Constant Initial Reservoir Temperature 49
5.2 Homogeneous Reservoir with Constant Thickness and Geothermal Gradient 52
5.3 Homogeneous Reservoir with Tapering Thickness and Constant Initial Reservoir Temperature 55
5.4 Homogeneous Reservoir with Divergent Thickness and Constant Initial Reservoir Temperature 59
5.5 Results Summary 62

6 Conclusions and Future Work 64

Nomenclature 65

References **67**

A Sample Input File **70**

B Analytical Solution **74**

C Additional Plots for Sensitivity Analyses **78**

C.1 Sensitivity to Porosity 78

C.2 Sensitivity to Formation Heat Conductivity 80

C.3 Sensitivity to Oil Density 82

C.4 Sensitivity to Specific Heat 84

C.5 Sensitivity to Thermal Expansion Coefficient 86

C.6 Sensitivity to Oil Viscosity 88

List of Tables

3.1 Summary of Grid Dimensions 7
3.2 Summary of Fluid and Rock Properties 11
3.3 Well Placement 12
3.4 Thickness Penetrated by the Well in the Reservoir 12
3.5 Well Dimensions 13
3.6 Initial Reservoir Thickness Estimates for Each Grid Type 14

4.1 Initial Reservoir Thickness Estimates for Each Grid Type 39

List of Figures

3.1 Constant Thickness Grid, with Homogeneous Properties 8

3.2 Tapering Thickness Grid, with Homogeneous Properties 9

3.3 Divergent Thickness Grid, with Homogeneous Properties 10

4.1 Temperature Profile Match with Porosity Uncertainty 20

4.2 Reservoir Thickness Prediction with Porosity Uncertainty for 49ft Reservoir 21

4.3 Reservoir Thickness Prediction with Porosity Uncertainty 22

4.4 Temperature Profile Match with Rock Conductivity Uncertainty . . . 23

4.5 Reservoir Thickness Prediction with Rock Conductivity Uncertainty for 49ft Reservoir 24

4.6 Reservoir Thickness Prediction with Rock Conductivity Uncertainty . 25

4.7 Temperature Profile Match with Oil Density Uncertainty 26

4.8 Reservoir Thickness Prediction with Oil Density Uncertainty for 49ft Reservoir 27

4.9 Reservoir Thickness Prediction with Oil Density Uncertainty 28

4.10 Temperature Profile Match with Specific Heat Uncertainty 29

4.11 Reservoir Thickness Prediction with Oil Specific Heat Uncertainty for 49ft Reservoir 30

4.12 Reservoir Thickness Prediction with Specific Heat Uncertainty 31
4.13 Temperature Profile Match with Thermal Expansion Coefficient Uncertainty 32
4.14 Reservoir Thickness Prediction with Thermal Expansion Coefficient Uncertainty for 49ft Reservoir 33
4.15 Reservoir Thickness Prediction with Thermal Expansion Coefficient Uncertainty 34
4.16 Temperature Profile Match with Oil Viscosity Uncertainty 35
4.17 Reservoir Thickness Prediction with Oil Viscosity Uncertainty for 49ft Reservoir 36
4.18 Reservoir Thickness Prediction with Oil Viscosity Uncertainty 37
4.19 Constant-Thickness with Geothermal Gradient Model 38
4.20 Sensitivity to Geothermal Gradient with Changing Derivative Models Temperature and Fixed kh 41
4.21 Reservoir Thickness Prediction with Geothermal Gradient, Changing Derivative Models Temperature and Fixed Kh 42
4.22 Reservoir Sensitivity to Geothermal Gradient with Derivative Models Temperature Similar to Prediction Model Temperature and Constant kh 44
4.23 Reservoir Thickness Prediction with Geothermal Gradient, Derivative Models Temperature Similar to Prediction Model Temperature and Fixed Kh 45
4.24 Reservoir Thickness Prediction with Geothermal Gradient, Derivative Models Temperature Similar to Prediction Model Temperature 46
4.25 Reservoir Sensitivity to Geothermal Gradient with Derivative Models Temperature Similar to Prediction Model Temperature 47

5.1 Partially Penetrated Constant-Thickness Model with Constant Initial Reservoir Temperature 50
5.2 Temperature Profile Match for Constant-Thickness Reservoir Model . 51
5.3 Reservoir Thickness Prediction for Constant-Reservoir Thickness Model 52
5.4 Partially Penetrated Constant-Thickness Model with Geothermal Gradient 53
5.5 Temperature Profile Match for Constant-Thickness Reservoir Model with Geothermal Gradient 54
5.6 Reservoir Thickness Prediction for Constant-Reservoir Thickness Model with Geothermal Gradient 55
5.7 Tapered Reservoir Model with Well 57
5.8 Temperature Profile Match for Tapered-Thickness Reservoir Model . 58
5.9 Reservoir Thickness Prediction for Tapered-Reservoir Thickness Model 59
5.10 Divergent Reservoir Model with Well 60
5.11 Temperature Profile Match for Divergent-Thickness Reservoir Model . 61
5.12 Reservoir Thickness Prediction for Divergent-Reservoir Thickness Model 62

C.1 Temperature Profile Match with Porosity Uncertainty: 84ft 78
C.2 Temperature Profile Match with Porosity Uncertainty: 163ft 79
C.3 Temperature Profile Match with Rock Conductivity Uncertainty for 84ft Reservoir 80
C.4 Temperature Profile Match with Rock Conductivity Uncertainty for 163ft Reservoir 81
C.5 Temperature Profile Match with Oil Density Uncertainty for 84ft Reservoir 82

C.6 Temperature Profile Match with Oil Density Uncertainty for 163ft Reservoir 83
C.7 Temperature Profile Match with Specific Heat Uncertainty for 84ft Reservoir 84
C.8 Temperature Profile Match with Specific Heat Uncertainty for 163ft Reservoir 85
C.9 Temperature Profile Match with Thermal Expansion Coefficient Uncertainty for 84ft Reservoir 86
C.10 Temperature Profile Match with Thermal Expansion Coefficient Uncertainty for 163ft Reservoir 87
C.11 Temperature Profile Match with Oil Viscosity Uncertainty for 84ft Reservoir 88
C.12 Temperature Profile Match with Oil Viscosity Uncertainty for 163ft Reservoir 89

Chapter 1

Introduction and Problem Statement

Reservoir thickness is an often overlooked properties in hydrocarbon exploration and production. Thickness is a critical property in determining the volumetrics of a reservoir which subsequently play into the quantification of the reserves portfolio of the operator. Production management and strategizing using material balance calculations require that the volume of the reservoir is known in order for a pressure and production rate match to be achieved. More often than not, such a match is obtained by altering the porosity without consideration for the possibility of an incorrect reservoir thickness assumption. In modern well test analysis where pressure transients are analyzed to determine reservoir properties such as permeability and skin, reservoir thickness is often assumed to be a known constant, attributed to the production interval intersected by the production string. In that case, the permeability of the reservoir is obtained from a permeability-thickness product, which in a constant-thickness assumption environment, would lead to errors in permeability

estimates.

In this work, temperature data was used as a matching parameter in an optimization problem to estimate reservoir thickness. Reservoir thickness estimation attempts were made in a partially penetrated constant-thickness reservoir, a tapering reservoir whose thickness thins away from the well and a divergent reservoir whose thickness increases away from the reservoir. Numerical methods were used to generate reservoir temperature profiles using Eclipse 300. The Levenberg-Marquardt algorithm was used to as a searching algorithm to determine the reservoir thickness which minimized the difference between the actual reservoir temperature and the model temperature.

Chapter 2 revisits published methods used for determining reservoir thickness. Chapter 3 goes through the methodology used in this work including reservoir and fluid properties, and the procedure undertaken to estimate thickness using Eclipse 300 and the Levenberg-Marquardt algorithm. Chapter 4 describes the investigation of the sensitivity to reservoir and fluid properties to the success of this method in estimating reservoir thickness. Discussion of results is presented in Chapter 5. Conclusions and recommendations for future work are presented in Chapter 6.

Chapter 2

Literature Review

During the early stages of exploration, seismic techniques are often used to determine the extent of a hydrocarbon reservoir and the thickness of the reservoir formation. Seismology utilizes the time it takes a sound wave to travel from a known sound source position, through the formation until it is reflected back due to impedance differences, into a sound receiver at a known position. The known sound source wavelet and recorded receiver wavelet are deconvolved to calculate the earth filter that the source wave travelled through, hence establishing an estimate of the reservoir rock thickness. Khare and Martinez [1] described a method to determine reservoir thickness using the ratio of seismic amplitudes from the same bedrock. They asserted the ratio method would work as it could isolate signatures caused by reservoir thickness from those caused by other reservoir properties. The downside of this method is that it works only for simple reservoir geometries. Kelly and Skidmore [2] suggested using trained neural networks with data obtained from common rock beds to determine bed thicknesses from seismic traces. However, to create an optimal network for this method to work, a large database would be required to train the networks

and such a database would itself need to be confirmed to be the absolute truth for each trace and subsequent thickness prediction to reduce uncertainty, which would be challenging to accomplish. Although seismic methodologies are very important in the first estimation of reservoir thickness to determine drilling location, they are rarely used once a hydrocarbon well begins production. Traditionally, well logs such as gamma ray coupled with density logs were used to determine the reservoir thickness. By utilizing the correlation between data provided by seismic methods, logs and cores, Marion et al [3] asserted that a better estimate of reservoir thickness could be obtained. Using pressure data, Aswad [4] found that total reservoir thickness contributing to flow could be determined from the intercept of the plot of total skin with the plot of skin due to partial penetration, on a skin versus total thickness plot, for a given wellbore radius. This was very useful, but limited only to partially-penetrated wells. Kabir and Joseph [5] also attempted to determine the reservoir permeability and subsequently reservoir thickness contributing to flow by splitting the permeability-thickness product obtained from pressure transient analysis. They derived a method that makes use of the reservoir diffusivity term and the slope on the plot of flowing downhole pressure versus sandface flowrate to determine reservoir thickness. Thickness-permeability product obtained from traditional pressure transient analysis was used to solve for thickness using permeability established from their method.

In this work, temperature measurements were used as a matching property to estimate reservoir thickness. It was assumed that temperature can be measured on the sandface of the borehole penetrated by the well by usage of distributed temperature sensors inserted behind the casing completion.

Temperature has been used as a quality control parameter to confirm pressure transients recorded in producing wells [6]. The utilization of temperature in determining

reservoir properties has recently been gaining momentum with more research confirming its usefulness in this field. Ramazanov and Parshin [7] used recorded temperature to determine the radius of the degassing zone in a oil- and water-saturated reservoir. Bahrami [8] used temperature data to determine the end of wellbore storage during a pressure transient analysis. Sui et al. [9] used temperature data along with pressure measurements to determine permeability, skin and damaged zone permeability and skin in a multilayered reservoir. Duru and Horne [10] established that temperature transient data can used to determine breakpoint in pressure data and damaged zone radius in the near-wellbore region. Zhang [11] used temperature data to determine vertical permeability information in deep reservoirs.

Is is evident from literature that temperature data can provide information about the reservoir as described by Zhang [11], Duru [10], Sui et al [9], and many others. The importance of the knowledge of reservoir thickness is evidenced by the amount of work in the area by Kabir and Joseph [5], Aswad [4] and many others using Seismic methods and pressure transient methods. In this work, we took advantage of the information carried by temperature data to try and estimate reservoir thickness.

Chapter 3

Methodology

This chapter outlines the reservoir grid properties and the fluid properties used to attempt the determination of reservoir thickness using temperature history. Also included is the optimization procedure and parameters used to reach the solution of reservoir thickness using temperature. A sample data file is included in Appendix A.

3.1 Grid Construction

Table 3.1 contains a summary of the grid dimensions used in the examples considered for this work. Three types of reservoir grids were used to investigate the utility of measured reservoir temperature in determining reservoir thickness: constant-thickness reservoir (Figure 3.1), tapered-thickness reservoir (Figure 3.2) and a divergent-thickness reservoir model (Figure 3.3). Three reservoir thicknesses (49ft, 84ft and 163ft) were used with each of the reservoir grid models. The grid dimensions were the same for all the models with 82 gridblocks in the x-axis, 82 gridblocks in the y-axis and 30 gridblocks in the vertical z-axis. Although the number of grids were

the same for all the models, they differed in the number of grids that contributed to flow. To allow grids in the model to contribute to flow and pore volume, specific grids were assigned a porosity of 23% and a permeability of 20md while the rest of the grids had zero permeability and 0.1% porosity. Of the 30 layers in the vertical axis, the top and the bottom five layers were treated as shales with zero permeability and 0.1% porosity, respectively simulating overburden and underburden. For the constant thickness grid models, the 20 layers between the overburden and underburden were assigned petrophysical properties (permeability=20md and porosity = 23%) that allowed for flow. The areal extent of all the reservoir grids were the same. Each of the gridblocks in the the grid models were 20ft-by-20ft in the x- and y-axes.

Table 3.1: Summary of Grid Dimensions

Grid type	**Constant-thickness model**			**Tapered-thickness model**			**Divergent-thickness model**		
Reservoir thickness	49 ft	84 ft	164 ft	49 ft	84 ft	164 ft	49 ft	84 ft	164 ft
x-y plane dimensions	82X82			82X82			82X82		
Gridblock thickness	2.45 ft	4.2 ft	8.15 ft	2.45 ft	4.2 ft	8.15 ft	2.45 ft	4.2 ft	8.15 ft
Overburden layers	layers 1-5			layers 1-5			layers 1-5		
Reservoir layers	layers 5-25			layers 5-25			layers 5-25		
Underburden layers	layers 26-30			layers 26-30			layers 26-30		
Model notes	Reservoir thickness is constant			Reservoir thickness only at said reservoir thickness in the middle where the well penetrates and then tapers off as if to model an anticline			Reservoir thickness only at said reservoir thickness by the no-flow boundaries. The reservoir is thinnest in the centre where the well penetrates and increases in thickness until the boundaries		

For the constant-thickness model reservoir, to vary the reservoir thickness the individual gridblocks in the 20 producing layers were changed simultaneously and equally until a desired total reservoir size (not grid size) was obtained. For instance, for the 84ft thick reservoir, each of the gridblocks in the 20 layers contributing to flow were a thickness of 4.2 ft which added to a total of 84ft over 20 layers. Similarly, the 49ft

reservoir had gridblocks with a thickness of 2.45ft while the 163ft had 8.15ft thick gridblocks. The over- and under-burden layers were not used in determining the gridblock thickness. However, they also were of the same thickness as the gridblocks contributing to flow.

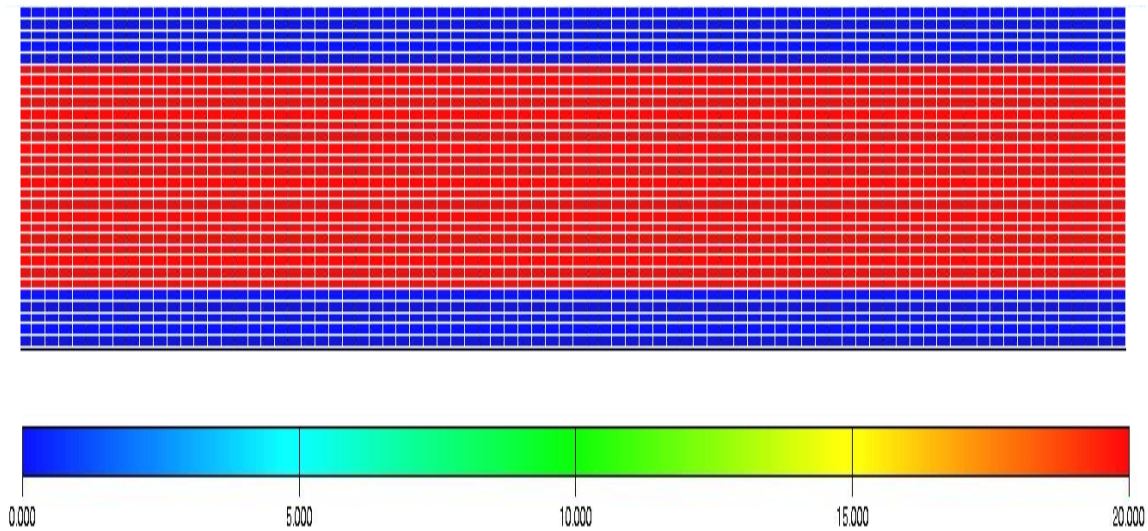

Figure 3.1: Constant Thickness Grid, with Homogeneous Properties

In the tapered-thickness model, the reservoir thickness was decreasing symmetrically away from the center of the reservoir. An "include" file was created in order to assign permeability and porosity to the specific grids which would produce the reservoir shape as shown in Figure 3.2. The permeability and porosity of the gridblocks contributing to flow were 20 md and 23%, respectively. All the other gridblocks had a permeability of zero and a porosity of 0.1%. The thickest portion of the reservoir, in the center of the grid, had the same thickness as the constant-thickness models (49ft, 84ft and 163ft) in the 20-layer producing interval. The difference between the

tapered model and the constant-thickness model was that the tapered model did not continue at the same thickness, but rather resembled an anticline reservoir by reducing in thickness every two grids away, on each side until it reached zero thickness on the outer-edge gridblocks, as illustrated in Figure 3.2. Similar methods as in the constant thickness models are used to alter the reservoir thickness (which refers to the thickest reservoir portion for the tapered model): the gridblock thicknesses were changed equally until the sum of the 20 layers in the middle of the grid equalled the desired reservoir thickness.

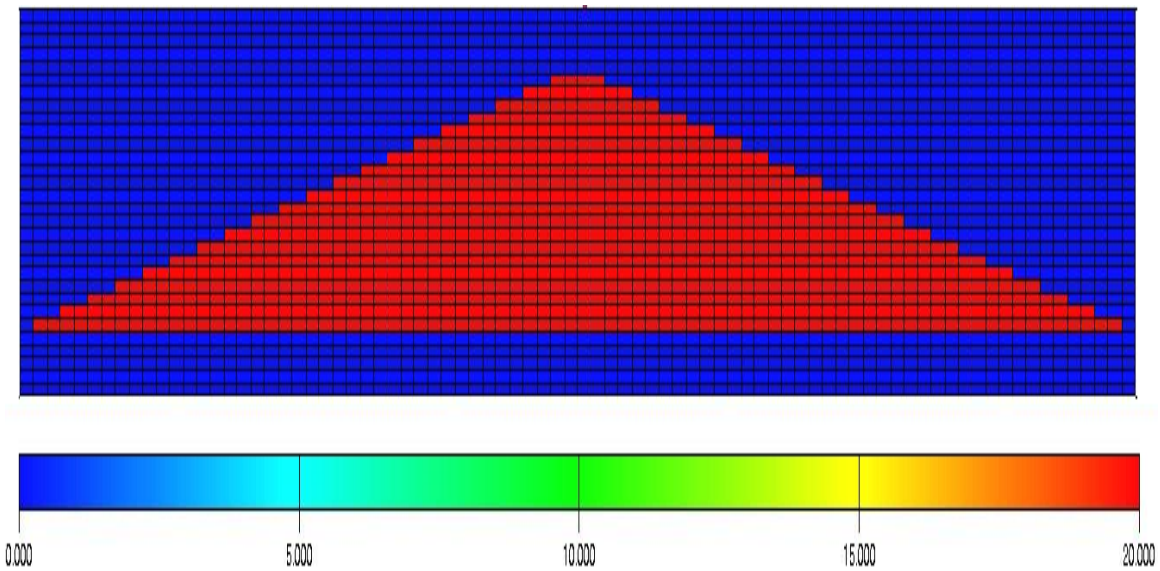

Figure 3.2: Tapering Thickness Grid, with Homogeneous Properties

Similar to the tapered-thickness model, the divergent-thickness model also contained an "include" file which was used to assign favorable permeability and porosity values to the specific gridblocks that provided the reservoir shape as shown in Figure 3.3. Unlike the tapered model, however, the divergent grid model is thinnest in the middle of the reservoir and thickens every three gridblocks away from the center in all

directions in the x-y plane until it is as thick as the constant-thickness models (49ft, 84ft or 163ft) in the three gridblocks on each side of the no-flow boundaries. In this manner, a 49ft, 84ft or 163ft divergent reservoir model refers to the maximum thicknesses in the reservoir. As in the tapered- and constant-thickness models, gridblock thickness were changed equally until the thickest portion of the reservoir reached the thickness of interest.

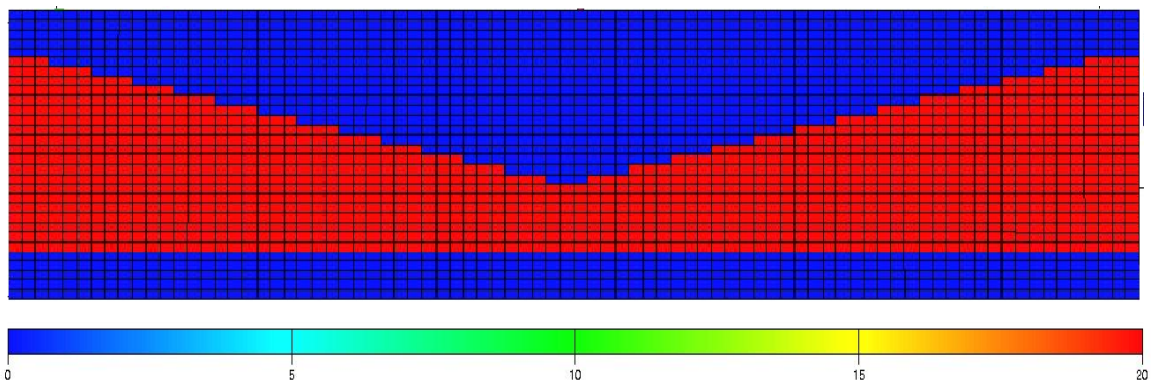

Figure 3.3: Divergent Thickness Grid, with Homogeneous Properties

3.2 Fluid and Rock Properties

The reservoir grids discussed in Section 3.1 were assumed to be homogeneous in petrophysical and fluid properties. The permeability for all the grids that contributed to flow was set at 20md. The porosity for all the grids contributing to flow was set at 23%. The permeability and porosity for the rest of grids in all the models were zero and 0.1%, respectively. Initial reservoir pressure was set at 3500 psi. Initial temperature was assumed constant at 240°F for each of the gridblocks in every model (no geothermal gradient) except for the model investigating sensitivity to geothermal gradient, which will be discussed in Chapter 4. Although the overburden

and underburden "shales" and the reservoir "sand" have been found to have differing heat conductivities [12], they were assumed in this investigation to have the same heat conductivity of 50 Btu/ft/day/°R. For simplicity, the oil saturation was set at 100%. The oil in the reservoir was set to have a viscosity of 3 cp, oil density of 40 lb/scf, specific heat of 3 Btu/lb/°R and a thermal expansion coefficient of 0.000178 $°R^{-1}$. Table 3.2 contains a summary of the essential rock and fluid properties used.

Table 3.2: Summary of Fluid and Rock Properties

Reservoir permeability	20	md
Reservoir porosity	23	%
Initial reservoir temperature	240	°F
Initial reservoir pressure	3500	psi
Oil saturation	100	%
Oil viscosity	3	cp
Oil density	40	lb/ft^3
Oil specific heat	5.00E-07	Btu/lb/°R
Oil thermal expansion coefficient	0.000178	$°R^{-1}$
Oil compressibility	5.00E-07	psi^{-1}

3.3 Well placement and Timestep

In all the grids in this work, there was only one well and the well was placed in block [42,42], which is the center of the reservoir. The depth of the well varied for the three grid mode types used. In the constant-thickness mode (Figure 3.1), the well was assumed to partially penetrate the reservoir. As discussed in Chapter 3.1, the first five layers of the grid were considered to be overburden. In each of the constant-thickness reservoir thicknesses (49ft, 84ft and 163ft), the well penetrated the first five layers of the reservoir, layers six through ten, in the vertical direction. This means that the actual thicknesses penetrated by the well in each grid with varying

reservoir thickness was different based on the dimensions of the grid (thickness of each gridblock) in that specific model. For instance, in the 84ft constant-thickness model, each of the gridblocks were 4.2ft thick, which means that the well penetrated a thickness of 21 ft.

The tapered-thickness reservoir (Figure 3.2) was fully penetrated from a grid in layer six through to a grid in layer 25, the thickest portion of the reservoir.

Similar to the tapered-thickness model, the divergent-thickness model (Figure 3.3) was fully penetrated. However, because its thickness is thinnest in the middle the layers contributing to flow in the region where the well was penetrating were layers 19 through layer 25. Table 3.3 contains the information on well placement for the grid block types used. Table 3.4 contains the data for the penetrated thickness in each well and Table 3.5 contains the well dimensions.

Table 3.3: Well Placement

Model type	Constant-thickness	Tapered-thickness	Divergent-thickness
X-coordinate	42		
Y-coordinate	42		
Top vertical coordinates	6	6	19
Bottom vertical coordinate	10	25	25

Table 3.4: Thickness Penetrated by the Well in the Reservoir

Model type	Constant-thickness			Tapered-thickness			Divergent-thickness		
Reservoir thickness (ft)	49	84	163	49	84	163	49	84	163
Well penetration thickness (ft)	12.25	21	40.75	49	84	163	17.15	29.4	57.05

Table 3.5: Well Dimensions

Wellbore radius	0.5	ft
Control oil rate	250	STB/d
Control pressure	50	psi

The simulator was run to obtain reservoir temperature during 10 days of production. In the first day of production, the time step used was 0.1 days. For the remainder of the test (9 days), the time step was one day. Time stepping in this manner provided 22 data points, including the initial temperature at time zero. All the models (actual reservoir, model reservoir and models used for sensitivity studies used the same time step).

3.4 Thickness Estimation Procedure

The purpose of this research was to use numerical simulation to determine reservoir thickness by matching temperature history. The problem at hand is an optimization problem. The simulator, Eclipse 300, with reservoir and fluid properties as described in the earlier sections of Chapter 3, was used to generate a temperature profile which formed the actual reservoir model's producing temperature to be matched. The block temperature of the first block intersected by the well was used for each of the three grid models discussed in Section 3.1. For both the constant-thickness model (Figure 3.1) and the tapered thickness model (Figure 3.2 the temperature of gridblock [42,42,6] was used while the temperature for the gridblock [42,42,19] was used for the divergent-reservoir model (Figure 3.3). Gridblock temperature was used as the distributed temperature sensor was assumed to be deployed outside of the casing string such that it could read sandface temperature.

The sequence of the process for determining reservoir thickness is described next. First we generated reservoir temperature profiles during production using the reservoir and fluid properties mentioned in Chapter 3, which would be the actual reservoir temperature. We generated a grid with the same number of gridblocks (82x82x30). The first grid layers were considered to be shale rock, which would be known from the fact that the well had to penetrate through some thickness of impermeable rock. For all three grid types, the initial reservoir thickness estimate equaled the amount of reservoir penetrated by the well, which can be seen in Table 3.6. Initially it was assumed that the thickness penetrated by the well was the total thickness. Because the grid has the same number of gridblocks as the actual reservoir, the thickness of each block in the model grid was the initial guess divided by 20 blocks. As there was no assumption of prior knowledge of the shape of the reservoir, a constant-thickness grid model was used to generate temperature profiles (using the temperature of the first block penetrated by the well) for all the grid types which would be matched to the actual reservoir temperature.

Table 3.6: Initial Reservoir Thickness Estimates for Each Grid Type

Grid type	Constant-thickness			Tapered-thickness			Divergent-thickness		
Reservoir thickness (ft)	49	84	163	49	84	163	49	84	163
Number of layers penetrated	5	5	5	20	20	20	7	7	7
Initial reservoir thickness estimation (ft)	12.3	21	40.8	49	84	163	17.2	29.4	57.1

Given a reservoir thickness estimate, Eclipse 300 would be initialized using the thickness estimate, then run to obtain reservoir temperature and which was compared to the actual reservoir temperature profile. The sum of the squares of the difference

between the actual reservoir temperature ($Tact$) and the model temperature ($Tmod$, the temperature obtained using the estimated reservoir thickness), Equation 3.1, needed to be below the threshold of 10^{-5}.

$$\sum_{i=1}^{22}(Tact_i - Tmod_i)^2 \tag{3.1}$$

The method used for optimization was the Levenberg-Marquardt (LM) algorithm, developed by Bandyopadhyay [13]. The LM algorithm requires the gradient and the Hessian in order to estimate the the next reservoir thickness based on the results from Equation 3.1. To calculate the gradient, 5ft were added and subtracted from the estimated reservoir thickness in each optimization step. Eclipse 300 was initialized and temperature profiles from the first block intersected by the well were obtained, a vector over the 10-day time period for the reservoir with addition of 5ft thickness and the reservoir with reduction of 5ft of the estimated thickness. The gradient vector was determined by Equation 3.2, where the denominator is the thickness change between the a reservoir thickness with five additional feet and that with five fewer feet, which is 10 ft in this case.

$$gradient = \sum_{i=1}^{22}\frac{(Tplus_i - Tminus_i)^2}{10} \tag{3.2}$$

where,

$Tplus$ = Temperature profile of the model with the thickness increased by five ft above the estimated reservoir thickness, and

Tminus = Temperature profile of the model with the thickness reduced by five ft above the estimated reservoir thickness

To calculate the derivative, the gradient (Equation 3.2) vector was multiplied with its transpose (Equation 3.3). With the gradient and the derivative, the LM algorithm estimated a reservoir thickness while minimizing the left hand side of Equation 3.1. The algorithm had two stopping criteria: it stopped if the reservoir thickness estimated gave a temperature profile that satisfied the condition for Equation 3.1 or if the algorithm reached 60 iterations, at which point the last thickness estimated was provided as the solution to the optimization problem. Because Eclipse 300 was initialized three times in each iteration to generate temperature profiles (for the predicted reservoir thickness, for the predicted reservoir thickness plus 5ft and for the predicted thickness minus 5ft), it took longer than 12 hours for each single run to converge. As expected for LM, the first few predictions had larger thickness changes with subsequent declines until convergence criteria was met. This meant that the algorithm would spend more iterations closer to the solution than to the initial guess. Typical number of iterations to convergence were 10 to 15 iterations.

$$hessian = gradient \times gradient^{-1} \tag{3.3}$$

3.5 Summary

Three reservoir grid types (Figure 3.1, 3.2 and 3.3), were used to investigate the utility of reservoir temperature in estimating reservoir thickness. The temperature of the first block intersected by the well was used due to the assumption that distributed temperature sensors deployed behind the casing were in place and could read sandface

temperature. Eclipse 300 was used to generate reservoir temperature profiles. The Levenberg-Marquard(LM) algorithm was used to minimize the error between the reservoir and the model temperature while estimating the reservoir thickness. With each iteration, Eclipse 300 was initialized three times to generate the temperature profile with the estimated reservoir thickness and the temperature profiles using the estimated thickness plus and minus 5ft in order to supply the LM algorithm means of calculating the gradient and the Hessian.

Chapter 4

Sensitivity Analysis

Using the constant-thickness model, Figure 3.1, sensitivity analyses were performed on the fluid and rock properties that contribute to the temperature solution as established in the derivation of the analytical model in Appendix B.

$$[(1-\phi)(\rho C_p)_f]\frac{\delta T}{\delta t} + (\rho C_p)_f.\mathbf{v}.\nabla.T = \nabla.\{[(1-\phi)k_s + \phi k_f]\nabla T\} + Q_{cond} + q_f^{'''} \quad (4.1)$$

The energy balance equation [14], Equation 4.1, used to derive the temperature solution is a function of:

Porosity,
Thermal conductivity of the formation,
Fluid density,
Formation density,
Specific heat capacity of fluid,

Thermal expansion coefficient,

Fluid viscosity,

Joule-Thomson coefficient, and

Heat capacity of the formation,

As we are trying to determine reservoir thickness given a temperature profile, we investigated the degree of knowledge required for the first seven properties in order for the backward model to estimate reservoir thickness to a certain degree of confidence based on the temperature profile of a known forward model. Constant-thickness reservoir models simulating a relative degree of variance in reservoir thickness from a 49ft reservoir representing a thin reservoir, an 84ft reservoir representing a medium-thickness reservoir and a 163ft reservoir representing a thick reservoir, were used. Each (uncertain) property was changed in each input model while all other properties were held constant, similar to the properties of the forward model, and the LM algorithm was used to determine reservoir thickness based on the best match to the forward model's temperature profile. The deviation from the actual thickness (49ft, 84ft or 163ft) was recorded and compared for the range of values of the uncertain property used. The sensitivity analyses results are discussed in each section corresponding to each property discussed in this chapter. Work performed on the 49ft thick reservoir is presented here. Additional plots for the 84ft and 163ft reservoirs can be found in Appendix C.

4.1 Sensitivity to Porosity

The model constructed to represent the reservoir has a porosity of 23%. To determine the tolerable error in porosity for reservoir thickness estimation, porosity values

ranging from 16% to 30% were used. In each instance, we changed the porosity value of the prediction model, and provided the LM algorithm an initial guess thickness equal to the thickness penetrated by the well as discussed in in Section 3.4. Figure 4.1 shows the best match temperature profiles for each of the porosity values investigated for actual reservoir thicknesses of 49ft for reservoir porosities of 16%, 20%, 28% and 30%. It can be seen from Figure 4.1 that even the best temperature profiles are not similar to the temperature profile of the actual reservoir.

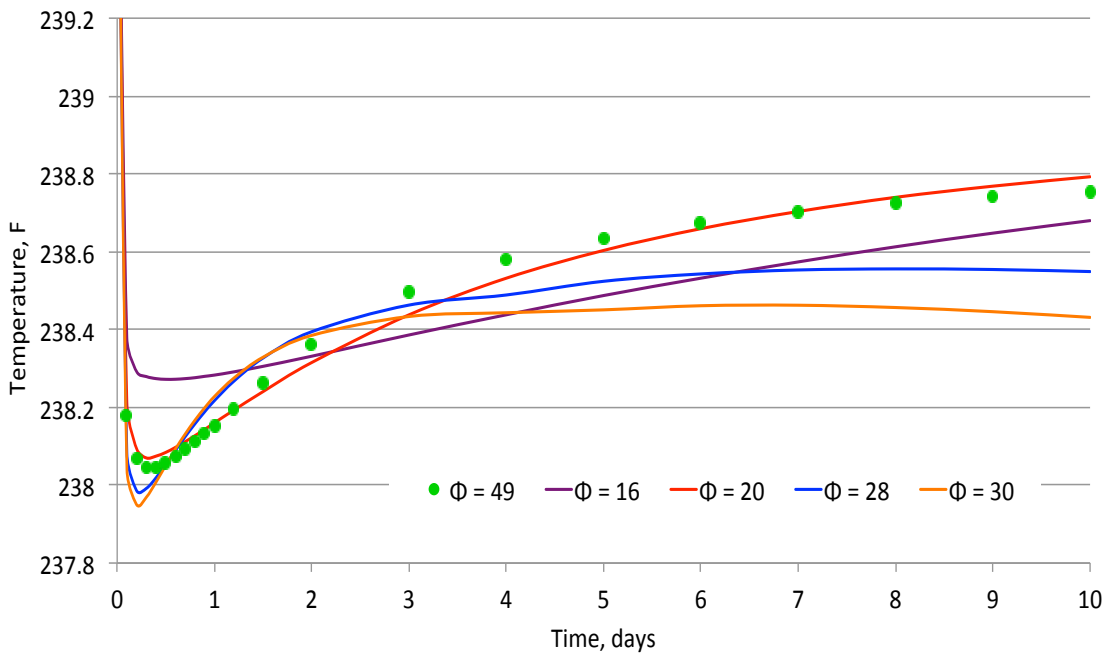

Figure 4.1: Plot showing the best match results in temperature profile with the uncertainty in reservoir porosity

Figure 4.2 shows the predicted thickness and error from the actual reservoir thickness for the 49ft reservoir. It can be seen that as the porosity decreases, the reservoir

thickness predicted increases and so does the error. As reservoir porosity increases, the predicted reservoir predicted decreases. The absolute error in reservoir thickness prediction increases as reservoir porosity increases, however, the same percentage error in porosity at higher porosities gives less error in reservoir thickness in comparison to lower porosities. For instance, the 16% porosity gives a thickness prediction error of 170% while the 30% porosity gives a thickness prediction error of 42% although both porosities are 30.4% different from the actual reservoir porosity of 23%.

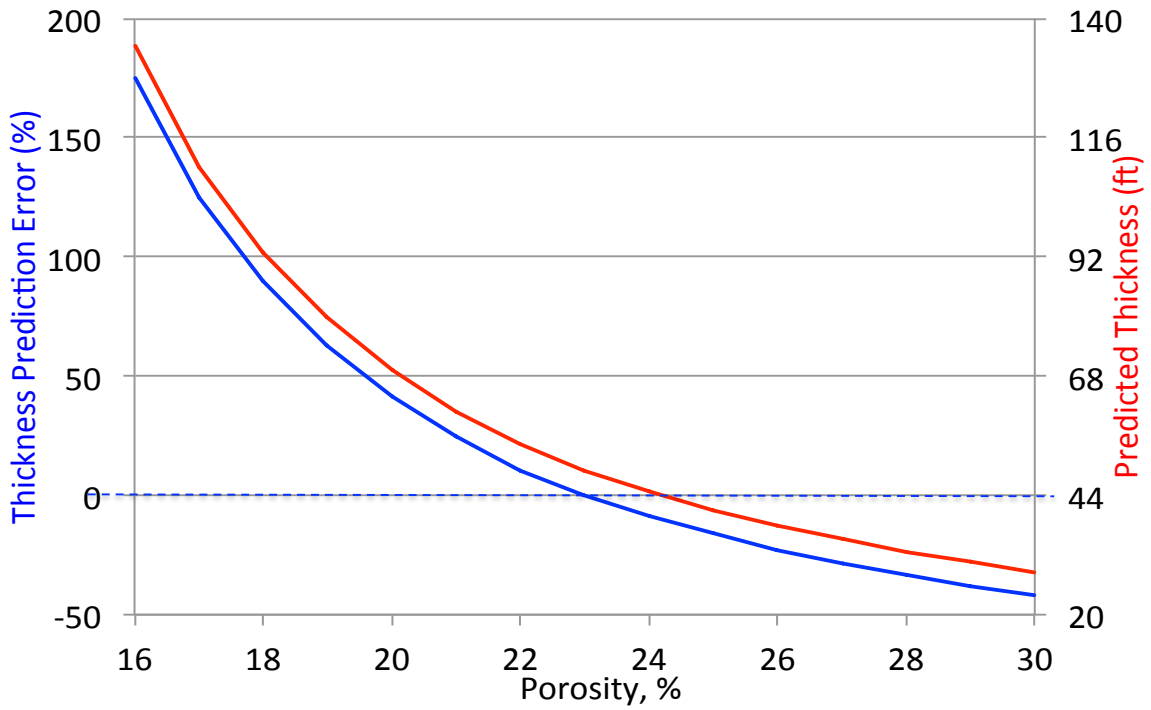

Figure 4.2: Plot showing the reservoir thickness predicted and its deviation (error) from the thickness of the actual reservoir for each of the porosity values investigated for the 49ft think reservoir

Figure 4.3 shows the predicted reservoir for each of the porosity values studied for all the actual reservoir thicknesses (49ft, 84ft and 163ft). For all the reservoir thicknesses

investigated, a knowledge in porosity within 5% of of the actual reservoir porosity is required for reservoir thickness prediction error to be within 20% of the actual reservoir thickness.

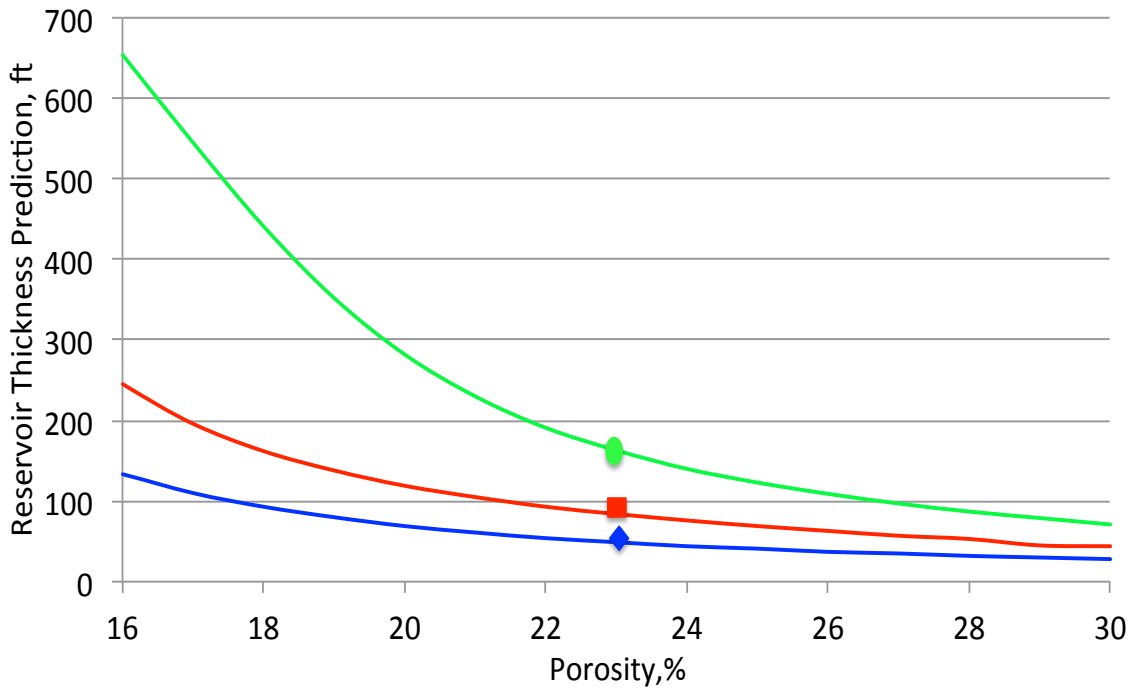

Figure 4.3: Plot showing the reservoir thickness predicted for each of the porosity values investigated for the 49ft, 84ft and 163ft thickness reservoir

4.2 Sensitivity to Formation Heat Conductivity

Although heat conductivity was assumed negligible in the derivation of the temperature solution in Appendix B, it still played a role in the heat transport in the model used in Eclipse 300. Prediction models with heat conductivities of 10,20,30,40,45,55,60

70,80, 90 and 100 BTU/ft/day/R were simulated to predict reservoir thickness compared to the actual reservoir heat conductivity of 50 BTU/ft/day/R. Figure 4.4 shows that the best match temperature profiles for the variable rock conductivity values vary in proximity to the actual value of the reservoir conductivity.

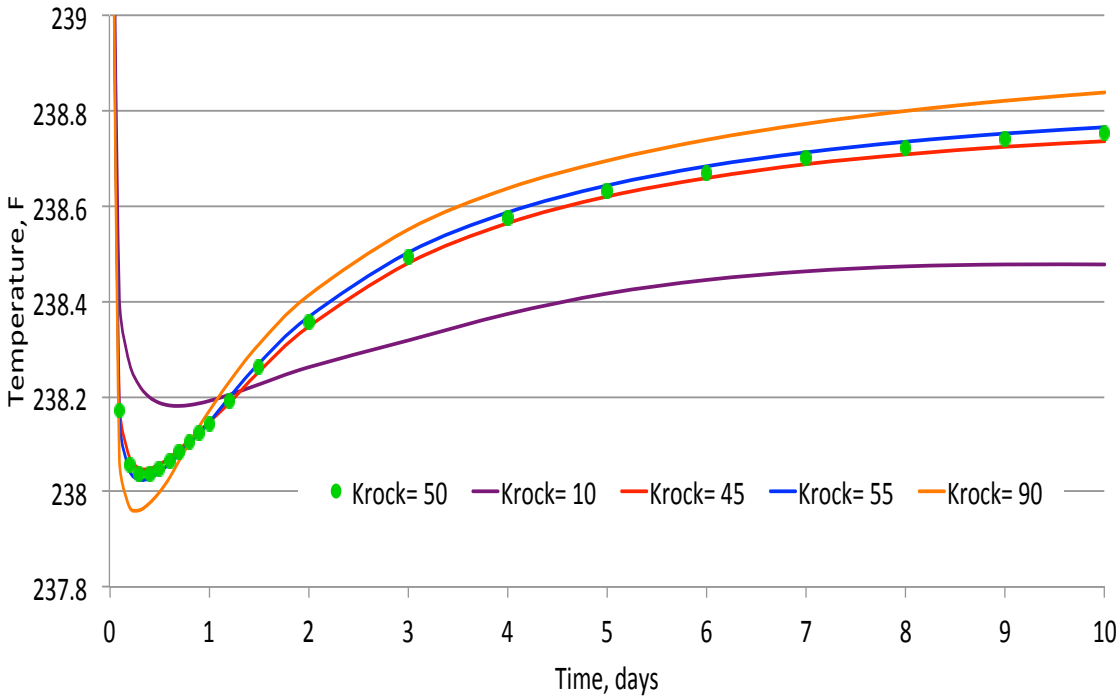

Figure 4.4: Plot showing the best match results in temperature profile with the uncertainty in reservoir conductivity

Figure 4.5 shows the predicted thickness and corresponding error from the actual reservoir thickness, for each rock conductivity value studied. It can be seen that the reservoir thickness prediction is within 10% for rock conductivity within 40% of the actual reservoir rock conductivity value. This is also true for the other reservoir thicknesses (84ft and 163ft) as can be seen in Figure 4.6. This means that the

precision with which the rock conductivity ought be known within for temperature models to provide a thickness solution within reasonable estimates is more flexible than that for porosity. This shows that conduction cannot be ignored altogether although the main mechanism for heat transport is advection.

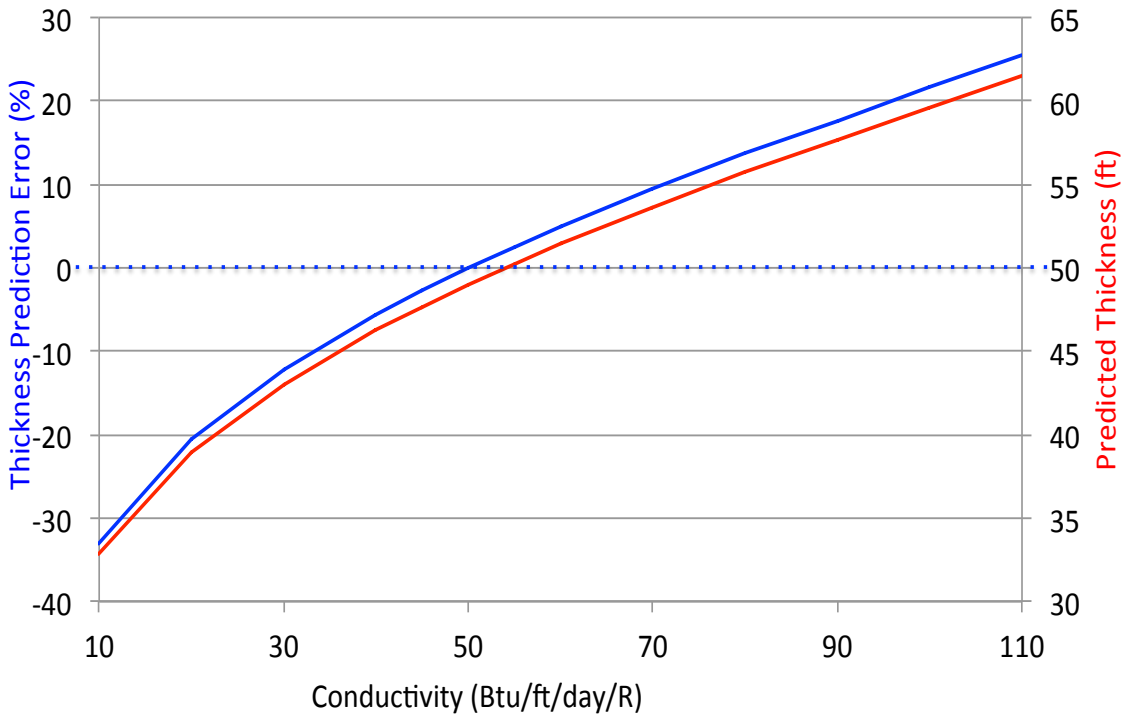

Figure 4.5: Plot showing the reservoir thickness predicted and its deviation (error) from the thickness of the actual reservoir for each of the rock conductivity values investigated for the 49ft think reservoir

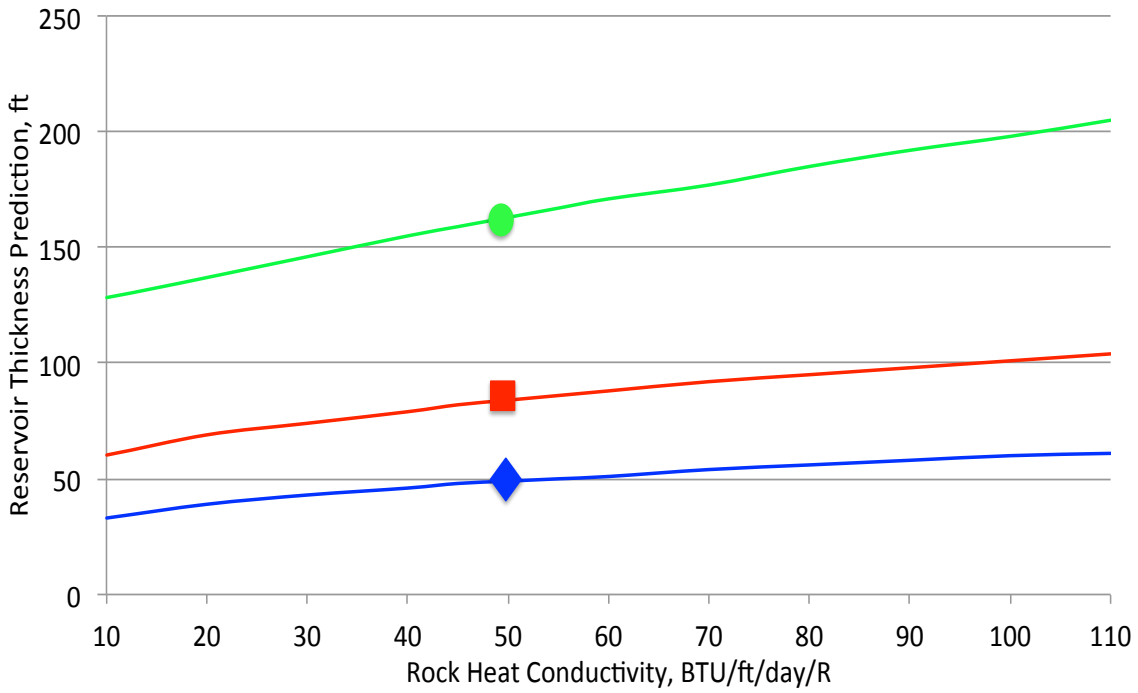

Figure 4.6: Plot showing the reservoir thickness predicted for each of the rock conductivity values investigated for the 49ft, 84ft and 163ft thickness reservoir

4.3 Sensitivity to Oil Density

Thickness prediction using temperature profiles for hydrocarbons with densities ranging from 10 to 80 API, representing a wide spectrum from heavy oil to ultralight oils, were compared against the actual reservoir thickness from a reservoir with a 40 API oil density. Please note that for ease of analysis, the oil density was changed to 40 API only for this "sensitivity to oil density" study. It is evident from Figure 4.7 that the temperature profile of the reservoir matched very well to the actual reservoir temperature profile.

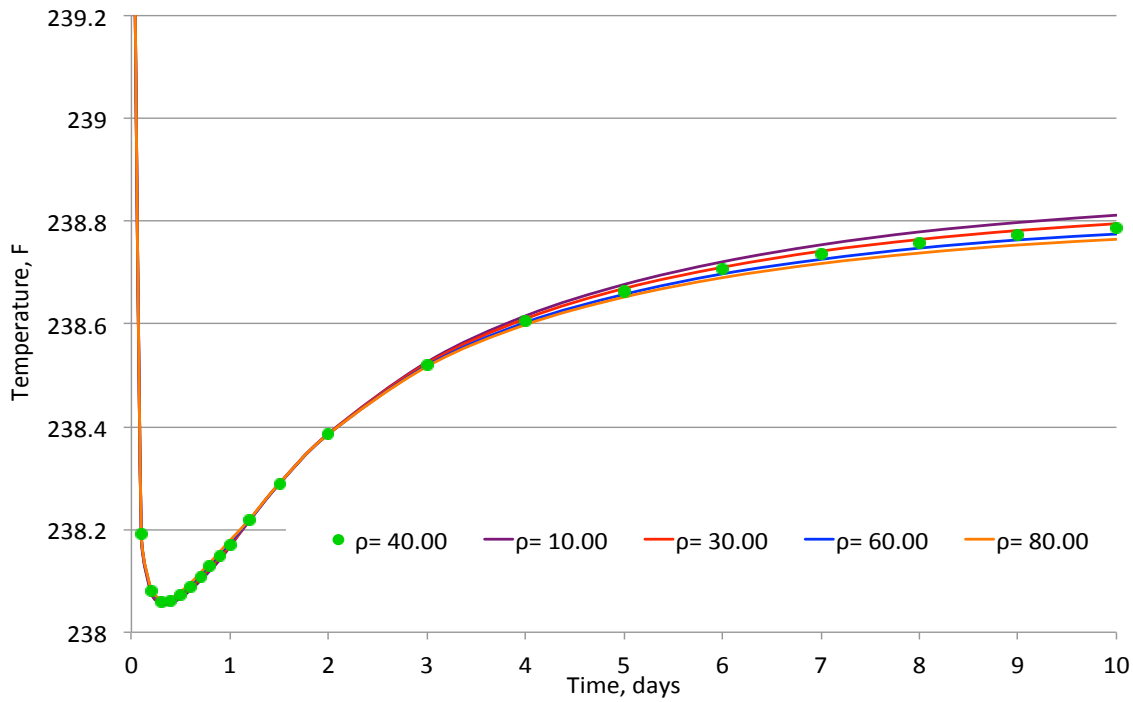

Figure 4.7: Plot showing the best match results in temperature profile with the uncertainty in oil density

Figure 4.8 shows the predicted thickness and relative error in reservoir thickness prediction as compared with the actual reservoir thickness. From Figure 4.8, the predicted thickness error for the 49ft reservoir is less than 3% for all oil density values studied. Figure 4.9 shows similar results for the 84ft and 163ft reservoirs. This shows that reservoir thickness is not a very strong function of oil density as an error in oil density of 100% gives an error in reservoir thickness prediction of 4%.

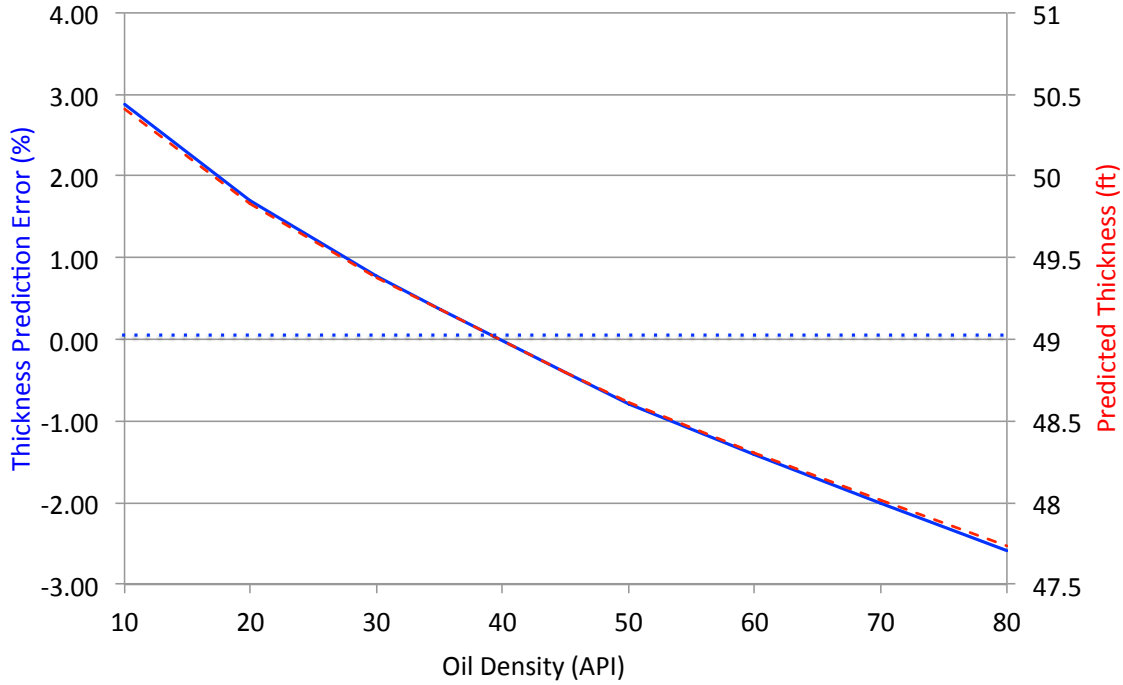

Figure 4.8: Plot showing the reservoir thickness predicted and its deviation (error) from the thickness of the actual reservoir for each of the oil density values investigated for the 49ft think reservoir

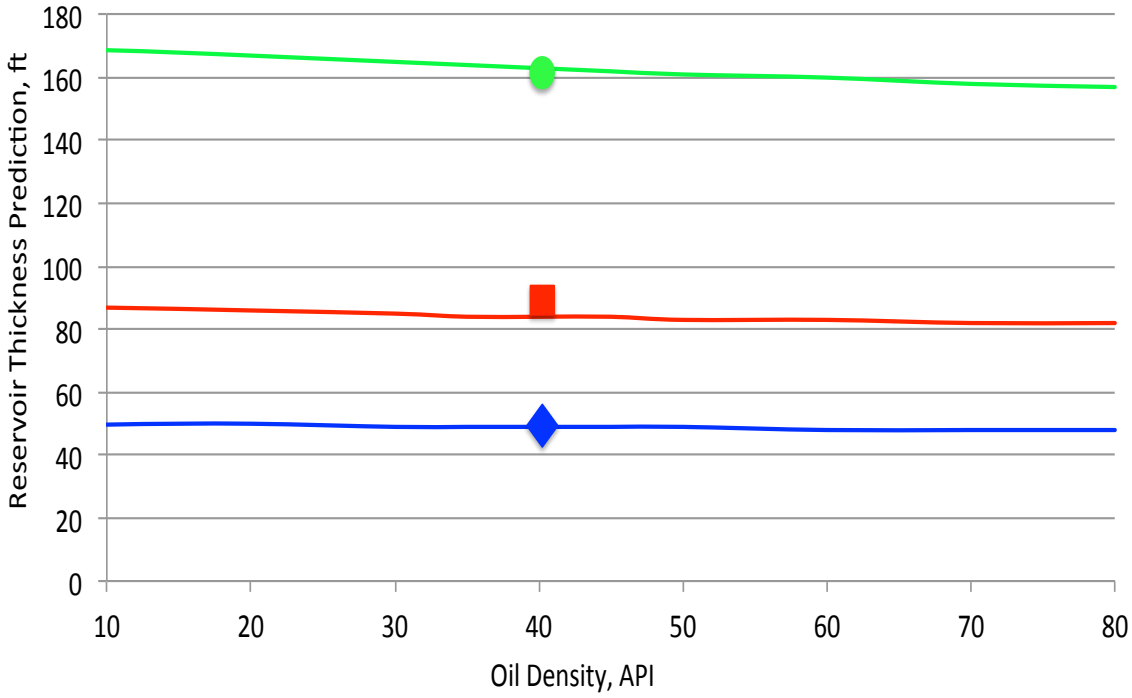

Figure 4.9: Plot showing the reservoir thickness predicted for each of the oil density values investigated for the 49ft, 84ft and 163ft thickness reservoir

4.4 Sensitivity to Specific Heat

Specific heat values of 1, 5, 15, 50 and 100 Btu/lb/°R were used to determine the range of values that would still provide an acceptable reservoir prediction error. The actual fluid specific heat was set at 3 Btu/lb/°R. Figure 4.10 shows the match results of attempts to predict the reservoir thickness while varying specific heat. The plots, even given the wide range of specific heat values, match very well to the actual reservoir's flowing temperature profile.

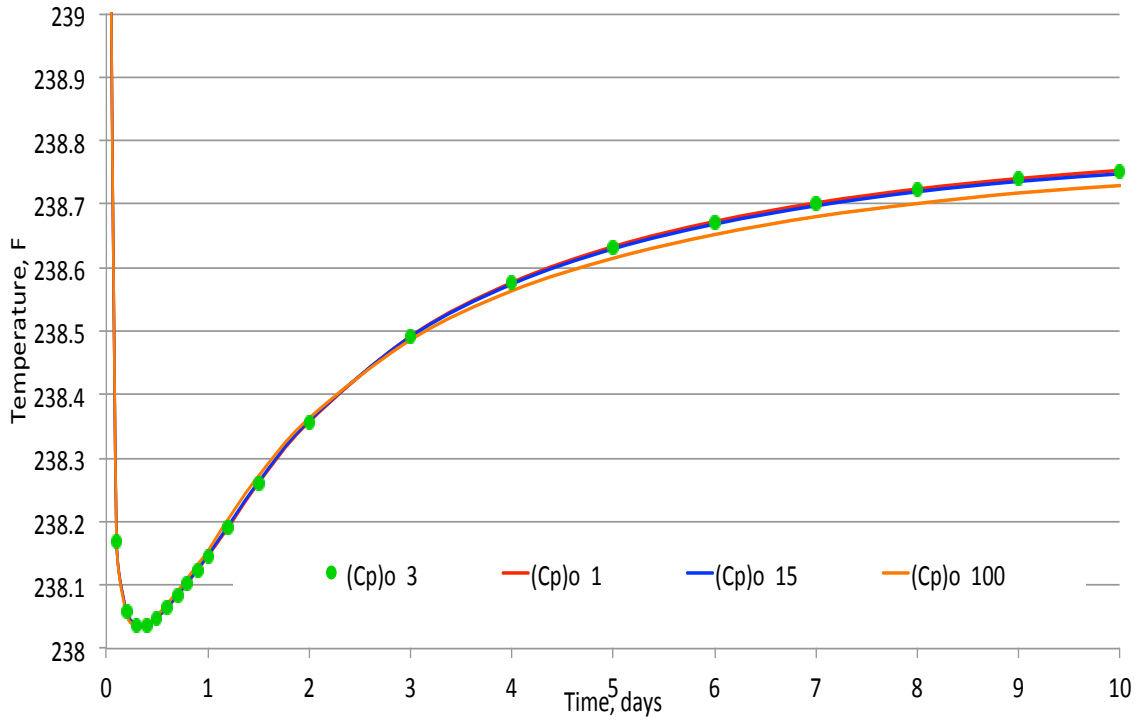

Figure 4.10: Plot showing the best match results in temperature profile with the uncertainty in oil specific heat

Figures 4.11 shows the reservoir thickness predicted and prediction error for the 49ft thick reservoir. 4.12 shows the predicted thickness for the 84ft and 163ft reservoirs. The prediction error for all the given reservoir thicknesses is less than 5% for a large specific heat error (>1000%). Similar to oil density (Section 4.3), reservoir thickness is not a strong function of oil specific heat in a single-fluid reservoir.

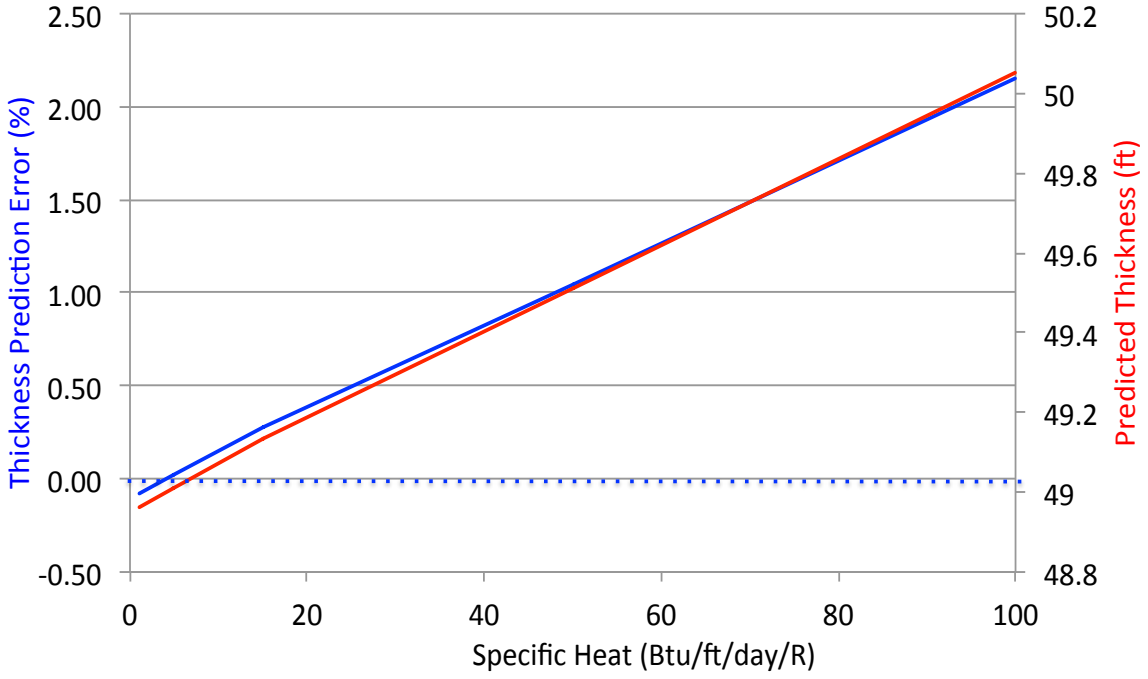

Figure 4.11: Plot showing the reservoir thickness predicted and its deviation (error) from the thickness of the actual reservoir for each of the oil specific heat values investigated for the 49ft think reservoir

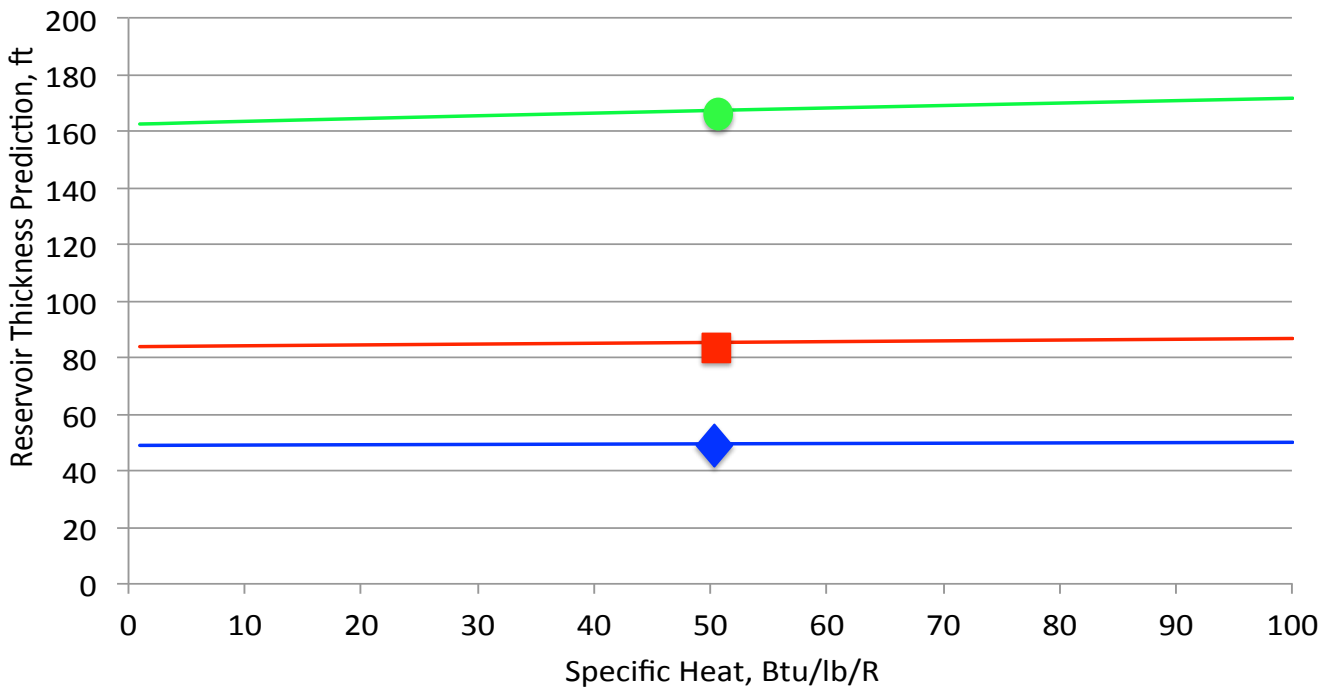

Figure 4.12: Plot showing the reservoir thickness predicted for each of the oil specific heat values investigated for the 49ft, 84ft and 163ft thickness reservoir

4.5 Sensitivity to Thermal Expansion Coefficient

Thermal expansion coefficient is a component of the advective form of temperature transport, which is the most dominant form of heat transport in porous media [15]. Thermal expansion coefficients ranging from 0.00001 to 0.001 R^{-1} were used to determine reservoir thickness based on temperature profiles from a reservoir with a specific heat of 0.000178 R^{-1}. Figure 4.13 shows the best match temperature profiles when the thermal expansion is unknown, which match very well to the reservoir temperature profile.

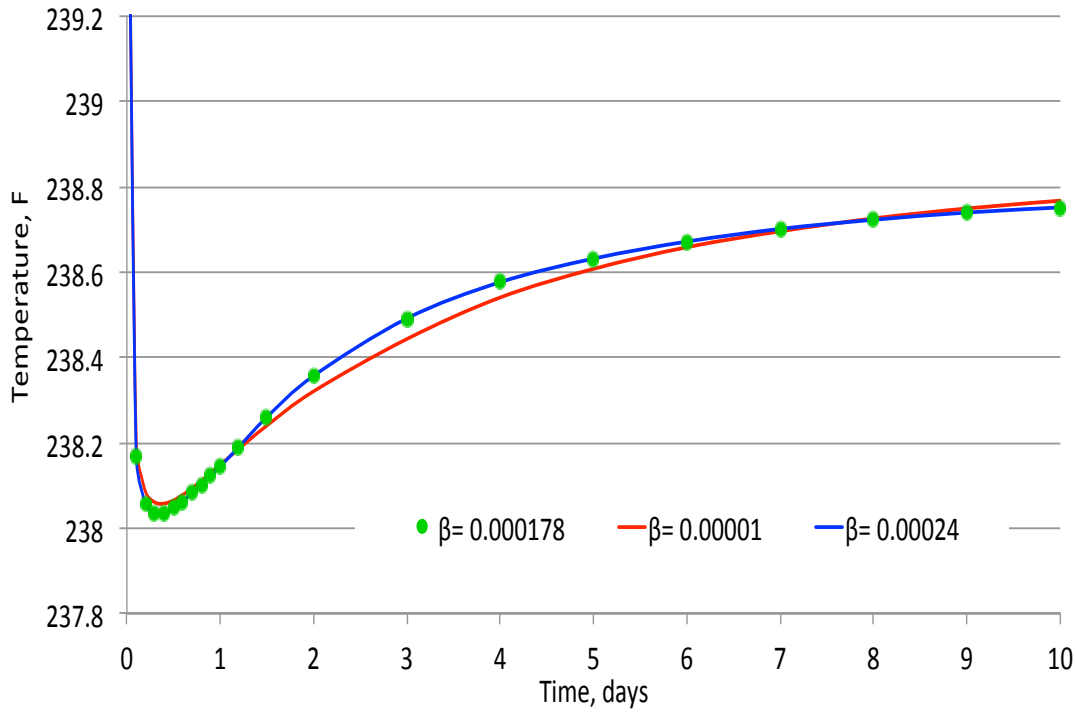

Figure 4.13: Plot showing the best match results in temperature profile with the uncertainty in thermal expansion coefficient for the 49ft thick reservoir

Figure 4.14 shows the predicted thickness and prediction error for the 49ft reservoir. The maximum error was observed to be at six percent for a thermal expansion coefficient error of 95%. Figure 4.15 shows the results for the 84ft and 163ft reservoirs also. This shows that reservoir thickness is not a strong function of specific heat coefficient.

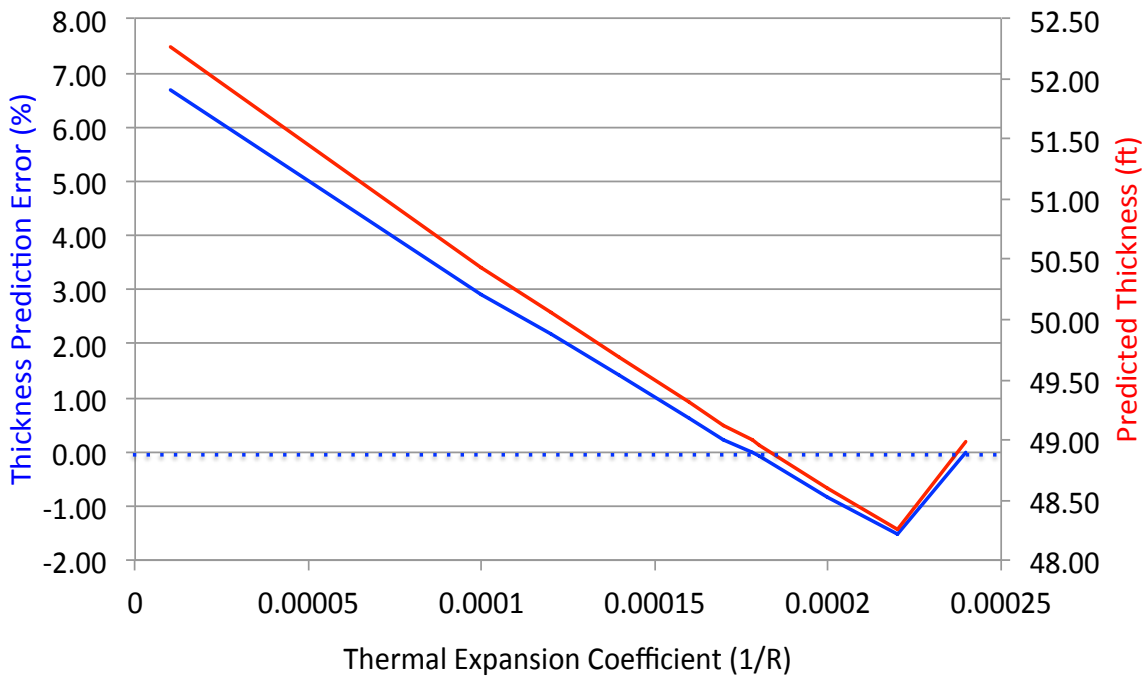

Figure 4.14: Plot showing the reservoir thickness predicted and its deviation (error) from the thickness of the actual reservoir for each of the thermal expansion coefficient values investigated for the 49ft think reservoir

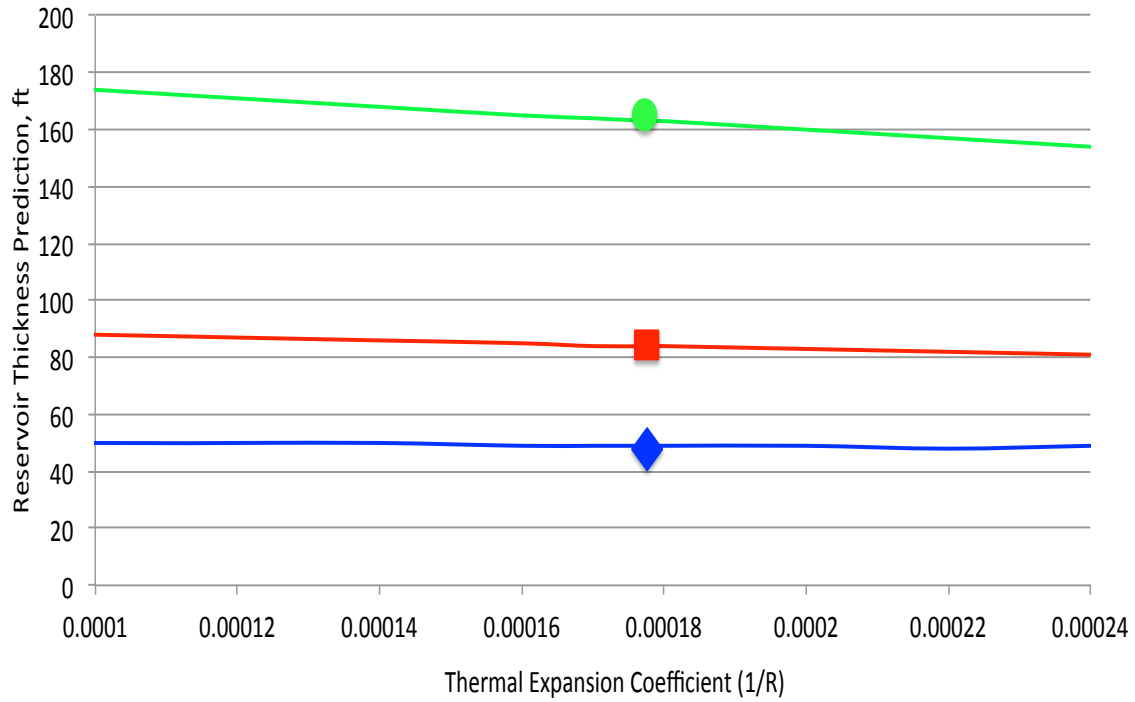

Figure 4.15: Plot showing the reservoir thickness predicted for each of the thermal expansion coefficient values investigated for the 49ft, 84ft and 163ft thickness reservoir

4.6 Sensitivity to Oil Viscosity

Although viscosity and density are oil properties that are very much related, this work only focused on sensitivities to oil viscosity and density separately. Therefore, although viscosity was varied in order to determine the requirement in its precision for reservoir thickness prediction, density was kept constant just like all the other reservoir and fluid properties not being investigated for this section. Figure 4.16 shows the best match temperature profiles for specific values of oil viscosity used for

a 49ft thick reservoir. It is evident from Figure 4.16 that there is not very much deviation from in the temperature profiles of the varied oil viscosity plots compared to the actual oil viscosity plot. The actual viscosity of the oil in the reservoir was five centipoise.

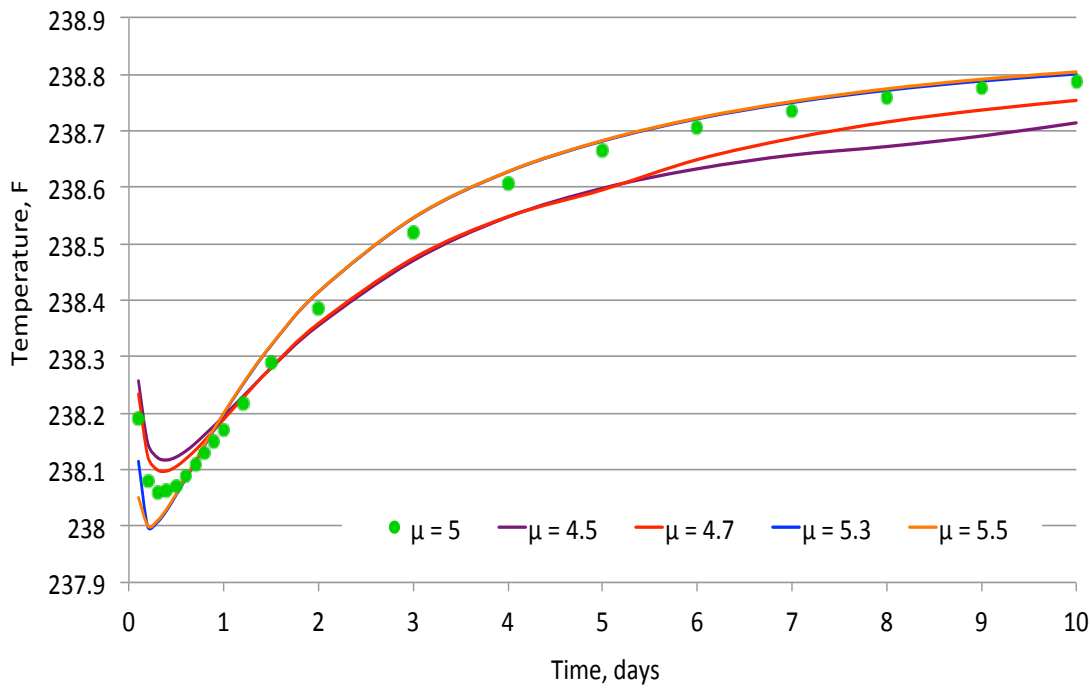

Figure 4.16: Plot showing the best match results in temperature profile with the uncertainty in oil viscosity for the 49ft thick reservoir

Figure 4.17 shows the predicted thickness and the associated error given uncertainty in oil viscosity for the 49ft reservoir. A maximum error of 15% is observed for a viscosity of 4.5 cp. These results were similar for the other reservoirs (84ft and 163) as well. Lower viscosity values give poorer reservoir prediction results compared to higher viscosity values. Figure 4.18 shows the predicted thicknesses for the 84ft and

163ft reservoirs. The larger the reservoir thickness, the higher the reservoir prediction error for the same oil viscosity uncertainty (40% reservoir thickness prediction error in the 163ft reservoir for 4.5 cp and 15% for the 49ft reservoir for 4.5cp).

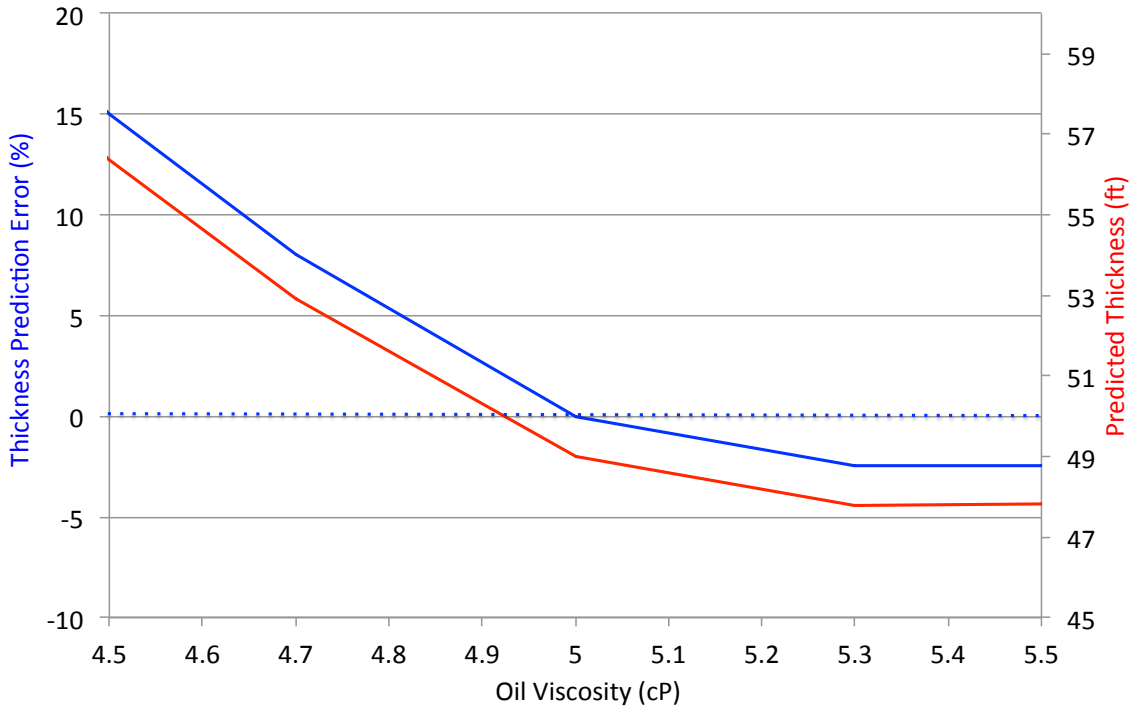

Figure 4.17: Plot showing the reservoir thickness predicted and its deviation (error) from the thickness of the actual reservoir for each of the oil viscosity values investigated for the 49ft thick reservoir

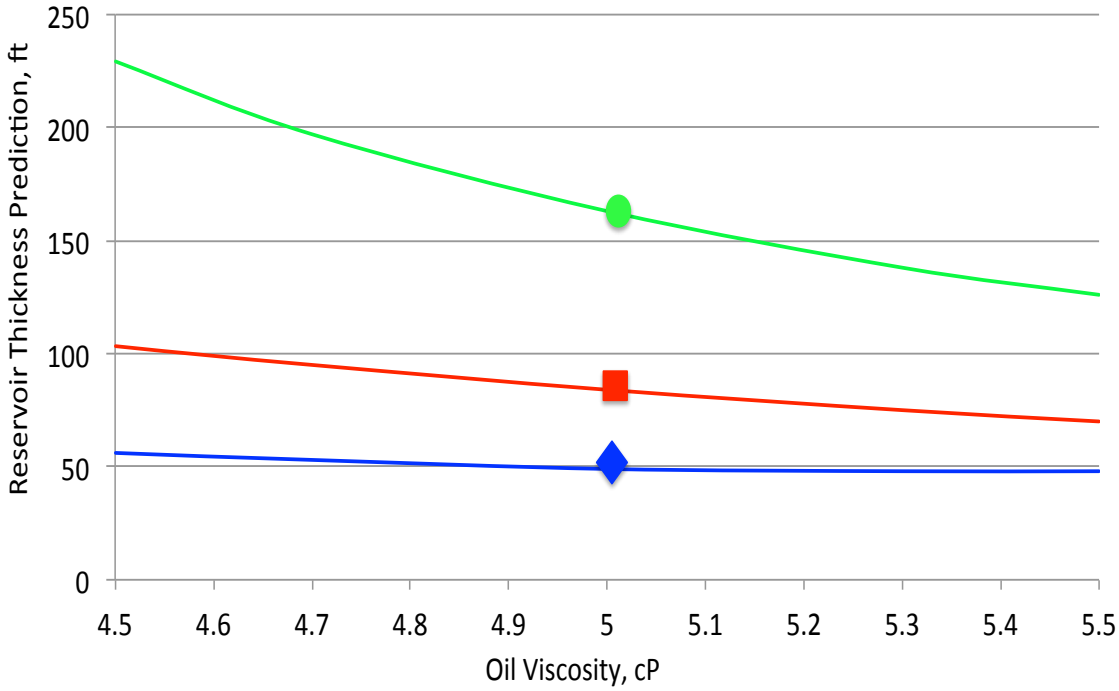

Figure 4.18: Plot showing the reservoir thickness predicted for each of the oil viscosity values investigated for the 49ft, 84ft and 163ft thickness reservoir

For a reservoir thickness of 49ft, oil viscosity within 10% of the actual oil viscosity will give a reservoir thickness error within 20% while it will give a reservoir thickness prediction error of 23% for the 84ft reservoir and 40% for the 163ft reservoir. This shows that reservoir thickness is a strong function of oil viscosity, more so at higher reservoir thicknesses.

4.7 Sensitivity to Geothermal Gradient

Because we were unable to automate a geothermal gradient at initial time using Eclipse 300, temperature values equivalent to a 20°F/1000ft geothermal gradient

were assigned to each layer with the assumption that the top layer was at a depth of 10000ft. This meant that the first layer had a temperature of 200°F and subsequent, deeper layers had temperature values calculated based on geothermal gradient and the thickness of each layer for the 49ft (dz=2.45ft), 84ft(dz=4.2ft) and 163ft (dz=8.15ft), where dz is the layer thickness. Figure 5.5 shows the grid used to model the sensitivity to geothermal gradient.

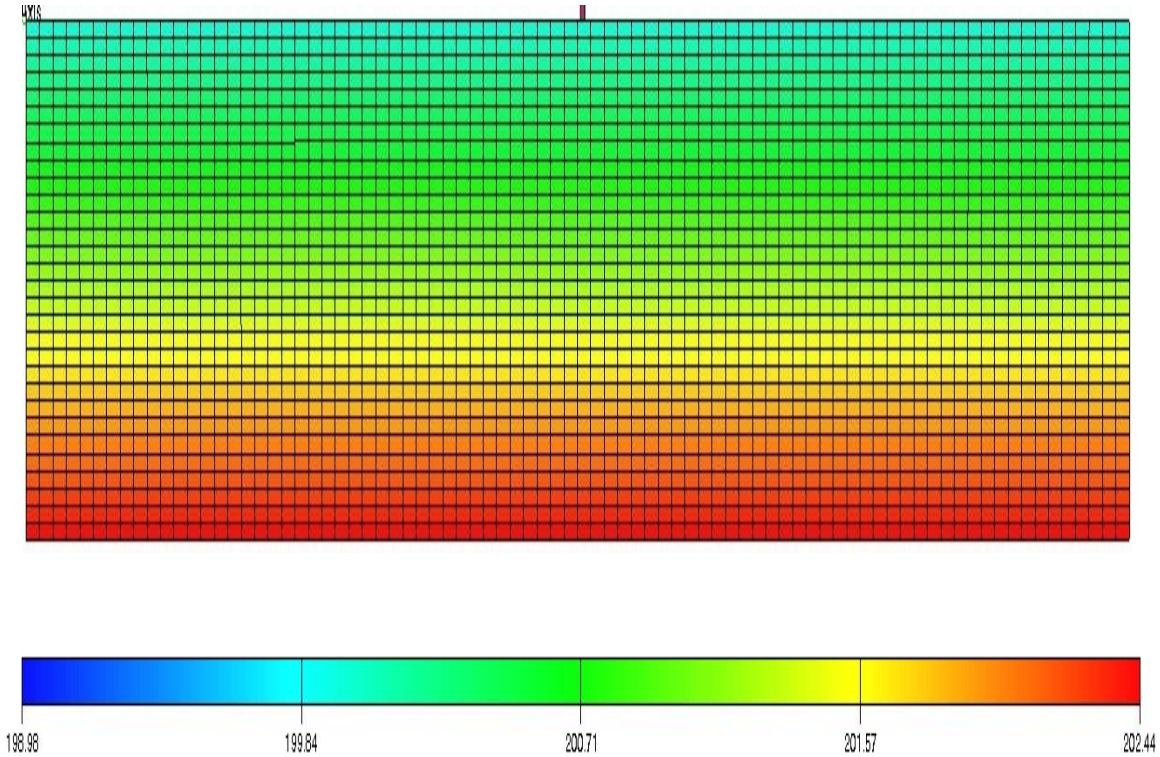

Figure 4.19: Grid model used for the study of reservoir-thickness prediction sensitivity to geothermal gradient

In each iteration the layer thickness was based on the predicted thickness of the reservoir which meant that the temperature for each layer changed with every iteration, keeping the geothermal gradient constant, until a best-match solution was

obtained. Due to the method used to determine the gradient used in the Levenberg-Marquardt algorithm (Section 3.4), the temperature for each of the models with an additional and reduced thickness was treated in two ways: One where the temperature was similar to the temperature of the thickness-prediction model given a geothermal gradient and another where the temperature changed with the thickness of the layers of the models used to obtain the gradient, given the same geothermal model. The permeability-thickness product was assumed known such that permeability was allowed to change as the predicted thickness changed. For the method where the temperature of the models used to determine the gradient was similar to that of the thickness-prediction model, an additional study was performed where the permeability was assumed to be known and only thickness changed with each iteration. For the method with a constant permeability-thickness, Table 4.1 shows the permeability-thickness products used for the three thicknesses used. To test the sensitivity to geothermal gradient, a model with an incorrect geothermal gradient of 19°F/1000ft was used against an actual geothermal gradient of 20°F/1000ft.

Table 4.1: Initial Reservoir Thickness Estimates for Each Grid Type

Reservoir thickness (ft)	Permeability-thickness product (md-ft)
49	49x20
84	84x20
163	163x20

4.7.1 Changing Temperature for Gradient-Calculation Models with Constant Permeability-Thickness Product

We were not able to match the 163ft model as it seemed to depend on the initial guess and never gave a solution that was more than 1ft different from the provided

initial thickness prediction, regardless of the value of the initial thickness provided. Due to time constraints, an investigation was not launched to determine the error with the geothermal gradient model for the 163ft reservoir.

The initial temperature profiles for the models used for calculating the gradient changed as their thickness was either greater or less than that predicted by the algorithm by 5ft. The permeability-thickness constant was as laid out in Table 4.1. It is evident from Figure 4.20 that even at a geothermal gradient of 19°F/1000ft thickness could be predicted within 5% error for the 49ft reservoir and within 25% for the 84ft reservoir as shown in Figure 4.21. As the thickness increases, the error in thickness prediction increases also, this is seen in Figure 4.21 for the 84ft although its temperature profile match as shown in Figure 4.20 was not very different from that of the actual reservoir temperature profile.

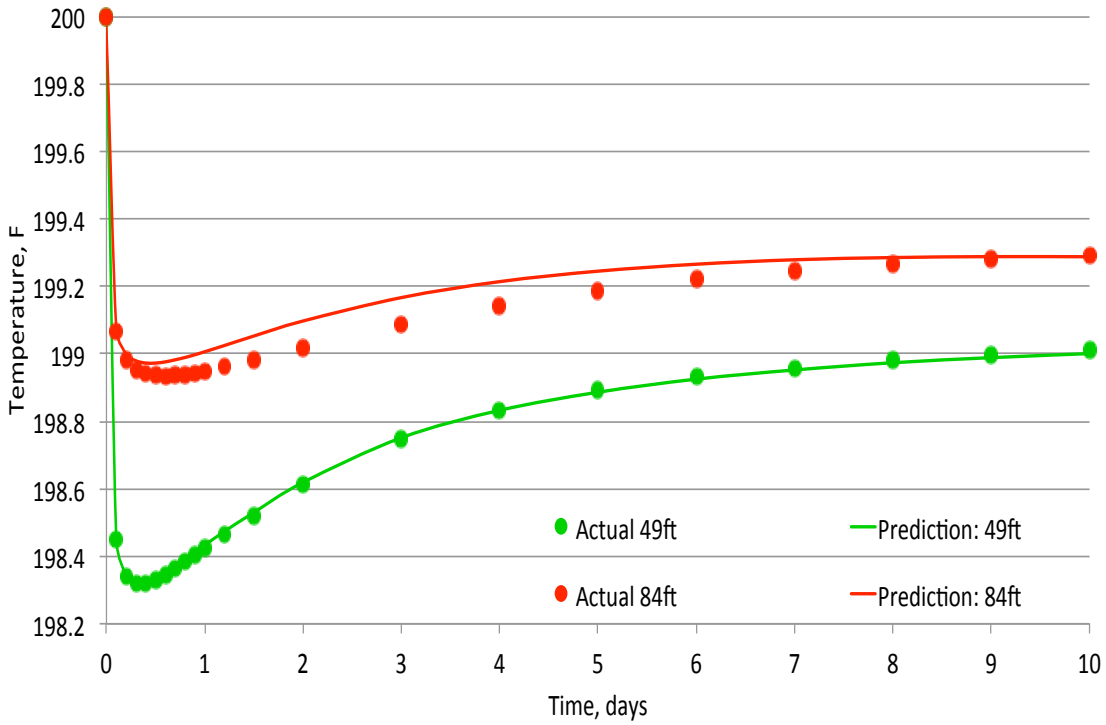

Figure 4.20: Plot showing the temperature match for the 49ft and 84ft reservoirs for a case where the grid models used to determine the gradient in the Levenberg-Marqaurdt algorithm have temperature different to the model with the predicted reservoir thickness based on their thickness and the geothermal gradient of 19°F/1000ft and a constant permeability-thickness product

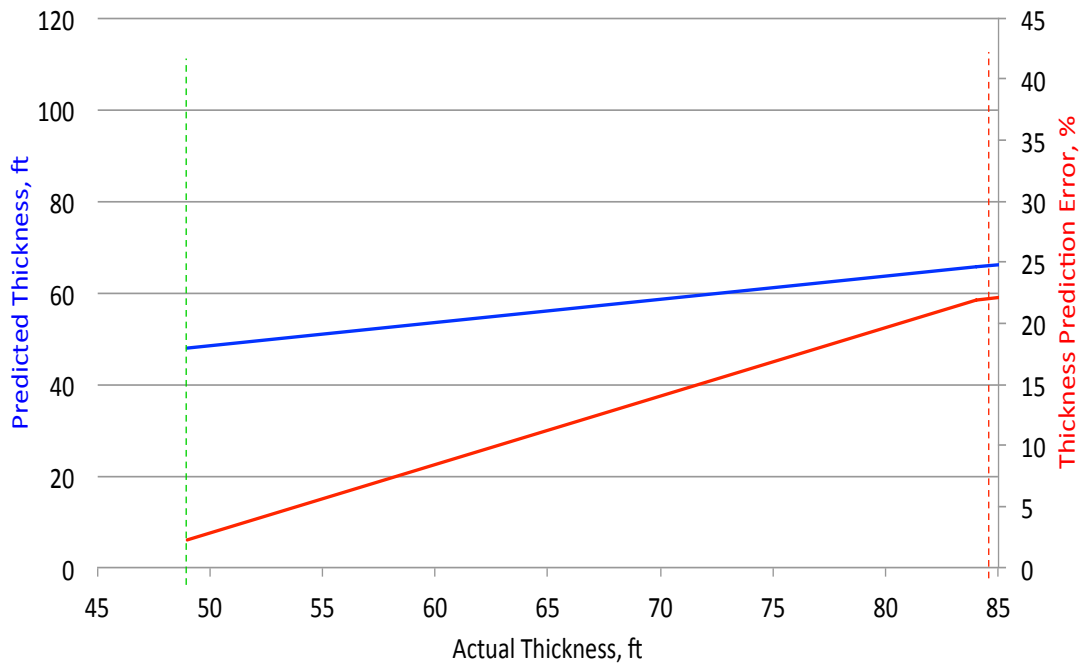

Figure 4.21: Plot showing the predicted reservoir thickness and subsequent errors for a case where the grid models used to determine the gradient in the Levenberg-Marqaurdt algorithm have temperature different to the model with the predicted reservoir thickness based on their thickness and the geothermal gradient of 19°F/1000ft and a constant permeability-thickness product

4.7.2 Gradient-Calculation Models with Temperature Similar to Thickness-Prediction Model Temperature and Constant Permeability-Thickness Product

We were not able to match the 163ft model as it seemed to depend on the initial guess and never gave a solution that was more than 1ft different from the provided initial thickness prediction. Due to time constraints, an investigation was not launched to

determine the error with the geothermal gradient model for the 163ft reservoir.

At 19°F/1000ft, the 49ft reservoir prediction model gave a reasonable match to the actual reservoir temperature profile as can be seen in Figure 4.22. Similarly, the 84ft reservoir prediction model gave a good match as can be seen in Figure 4.22. The predicted thicknesses and associated errors for both the 49ft and 84ft reservoirs are shown in Figure 4.23. The error for the 49ft reservoir is within 5% and that for the 84ft reservoir is within 10%. This shows that for both the 49ft and 84ft reservoirs, reservoir thickness can still be estimated sufficiently even when the geothermal gradient estimation is off by 1°F/1000ft.

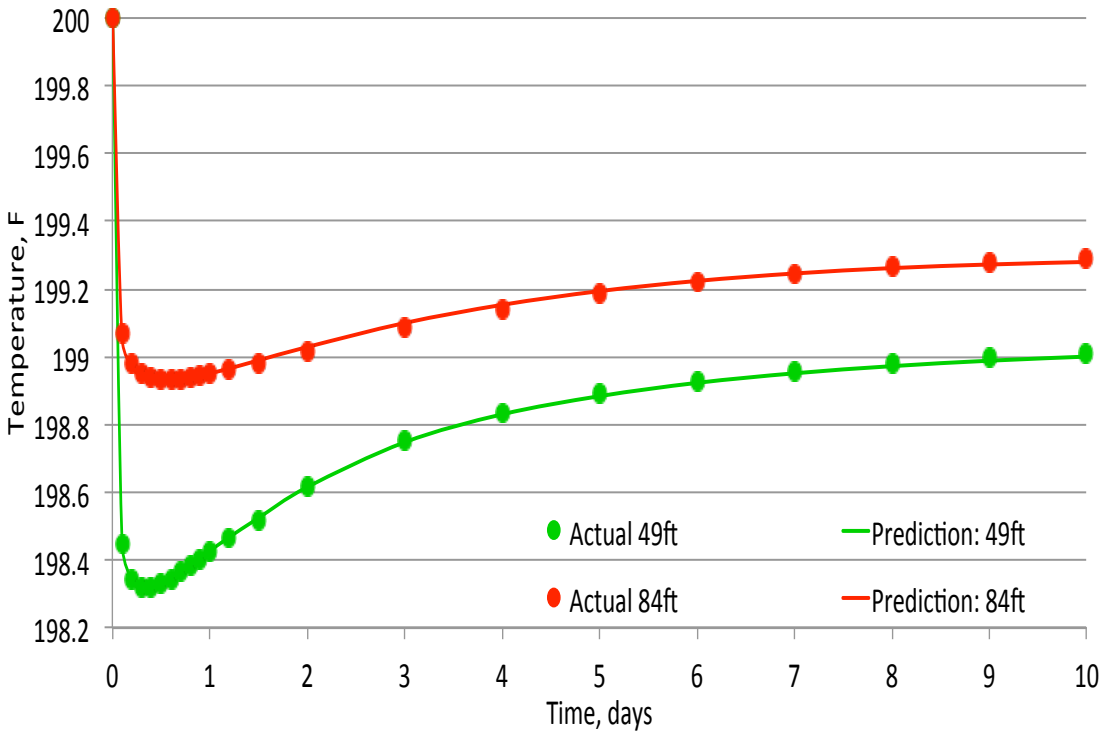

Figure 4.22: Plot showing the temperature match for the 49ft and 84ft reservoirs when the temperature of the grid models used to determine the gradient in the Levenberg-Marqaurdt algorithm have the same temperature as the model with the predicted reservoir thickness and a constant permeability-thickness product

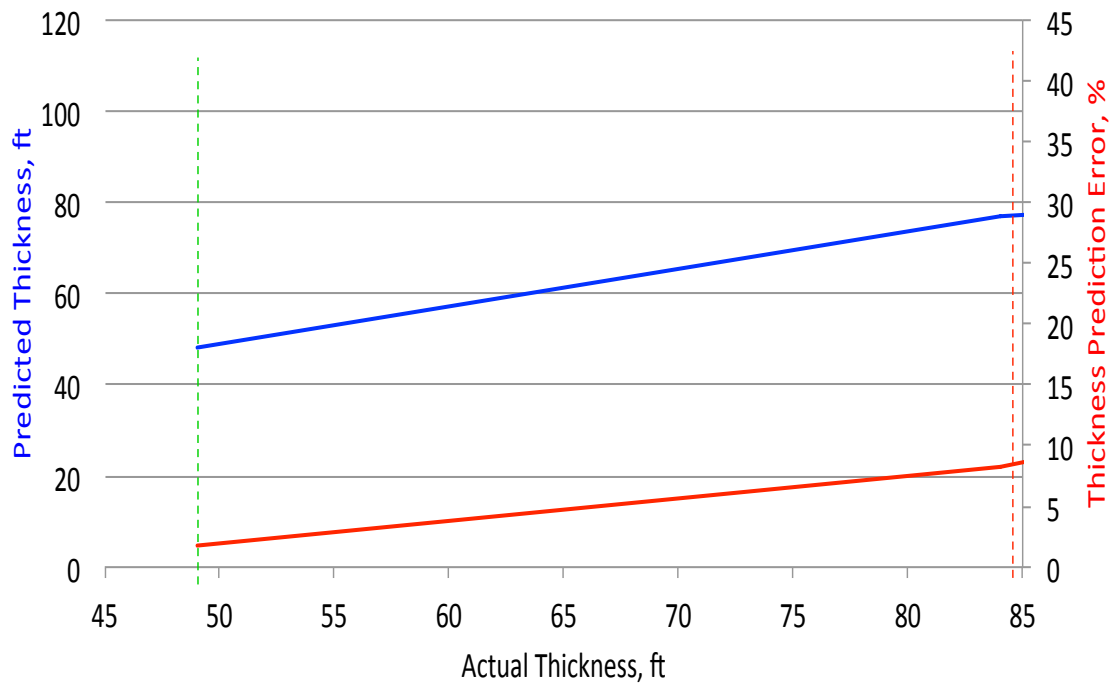

Figure 4.23: Plot showing the predicted reservoir thickness and subsequent errors when the grid models used to determine the gradient in the Levenberg-Marqaurdt algorithm have similar temperature profile as the model with the predicted reservoir thickness and a constant permeability-thickness product

4.7.3 Gradient-Calculation Models with Temperature Similar to Thickness-Prediction Model Temperature and Constant Permeability

With the constant permeability models where only thickness changed with each iteration, all three reservoir models gave a reservoir thickness prediction with 3% of the actual reservoir thickness, as shown in Figure 4.24. The temperature profiles for the 49ft, 84ft and 163ft reservoir prediction models with a geothermal gradient of

19°F/100ft are very similar to the actual reservoir temperature profiles with geothermal gradient equal to 20°F/1000ft, as can be seen in Figure 4.24. This shows that with a known permeability, a geothermal gradient which is uncertain within 5% of actual reservoir geothermal gradient should not pose an issue when temperature is used to determine reservoir thickness.

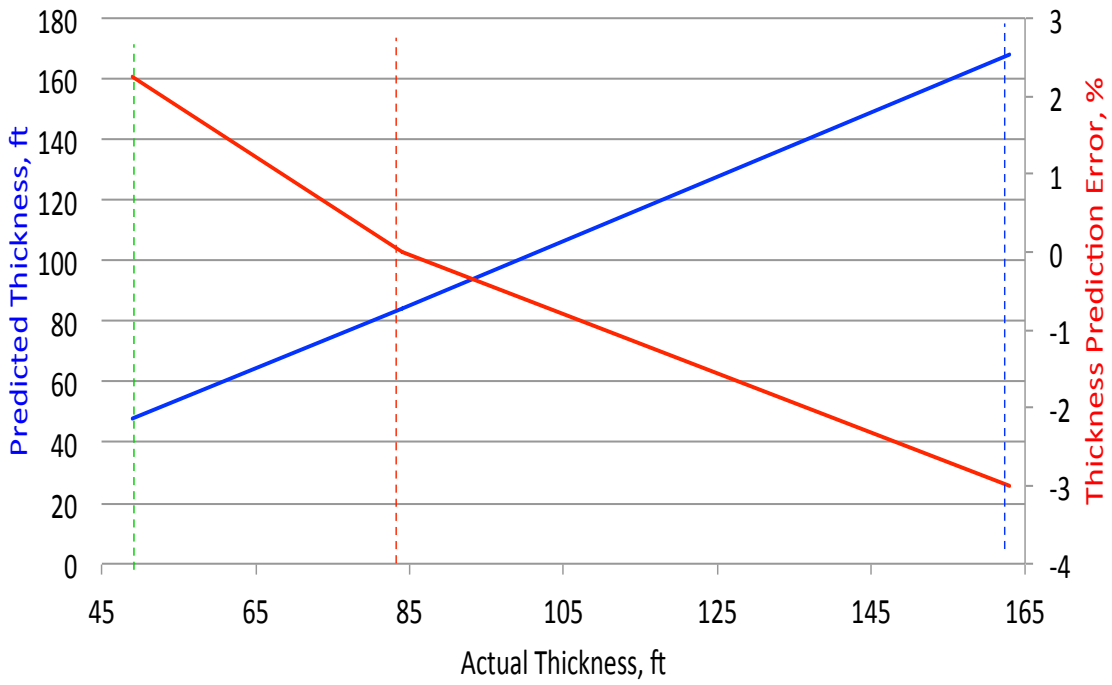

Figure 4.24: Plot showing the predicted reservoir thickness and subsequent errors when the grid models used to determine the gradient in the Levenberg-Marqaurdt algorithm have similar temperature profile as the model with the predicted reservoir thickness and a constant permeability

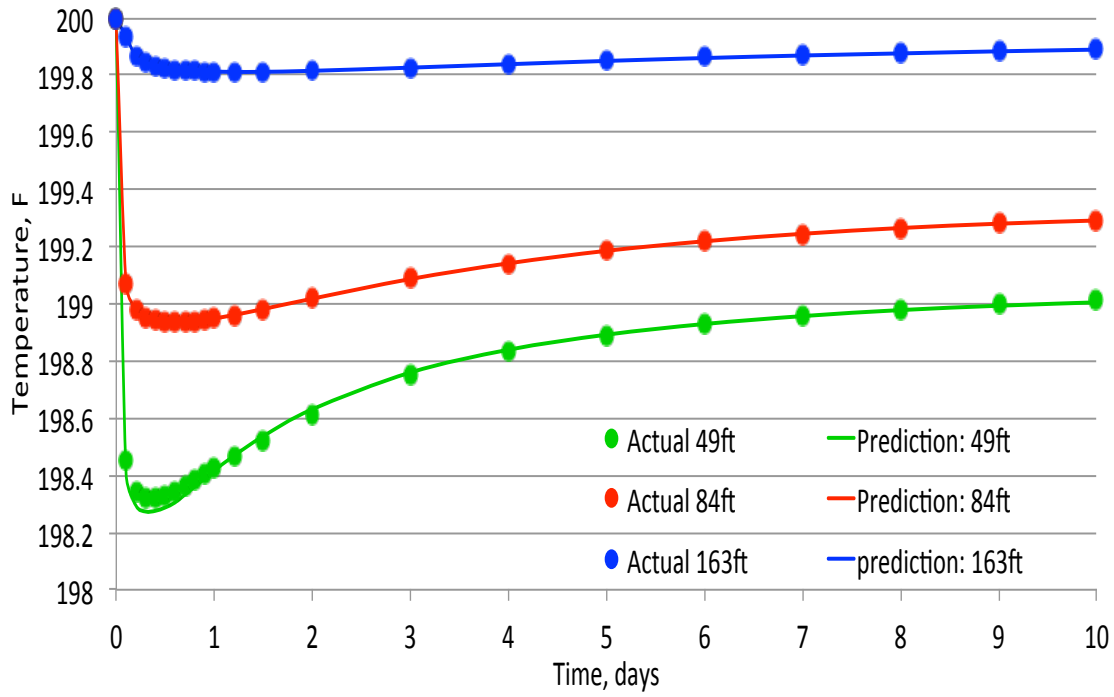

Figure 4.25: Plot showing the temperature match for the 49ft, 84ft and 163ft reservoirs when the temperature of the grid models used to determine the gradient in the Levenberg-Marqaurdt algorithm have the same temperature as the model with the predicted reservoir thickness and a constant permeability

4.8 Summary

The ability to predict reservoir thickness was very dependent on the knowledge of formation porosity, heat conductivity and oil viscosity. With large errors in oil density, specific heat and thermal expansion coefficient, we were still able to predict reservoir thickness. Therefore, the precision requirement for porosity, conductivity and viscosity in reservoir thickness determination is greater than the precision required for oil density, specific heat and thermal expansion coefficient. Sensitivity to

geothermal gradient seems negligible for small changes in geothermal gradient when all other properties including permeability are known.

Chapter 5

Results and Discussion

5.1 Homogeneous Reservoir with Constant Thickness and Constant Initial Reservoir Temperature

Figure 5.1 shows a schematic representative of the partially-penetrated reservoir used for this study. Figure 5.2 shows the results from matching the 49ft, 84ft and 163ft thickness reservoirs. The models' temperature profiles matched the actual reservoir temperature profile almost exactly. Figure 5.3 shows the predicted thickness and the associated error. The reservoir thickness prediction error is less than 0.1% for all three thicknesses investigated. This shows that for a partially-penetrating well, temperature can be used to determine the extent of reservoir thickness given that all other properties are known.

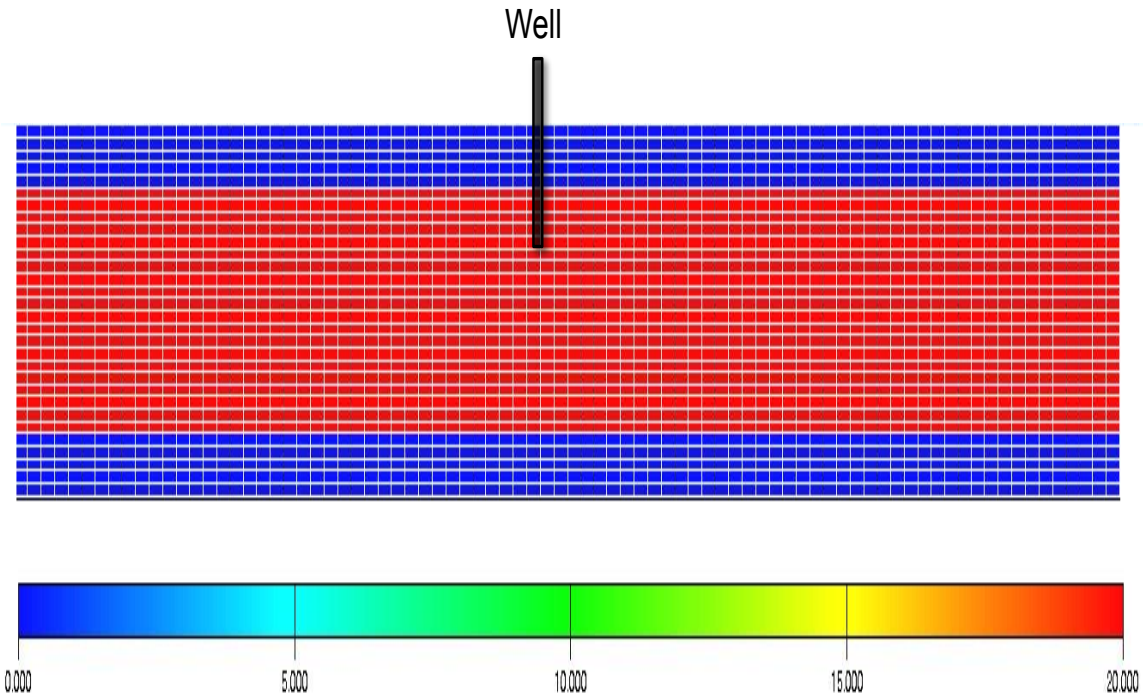

Figure 5.1: Grid for the partially penetrated, constant-thickness reservoir used to determine the reservoir thickness in a homogeneous reservoir

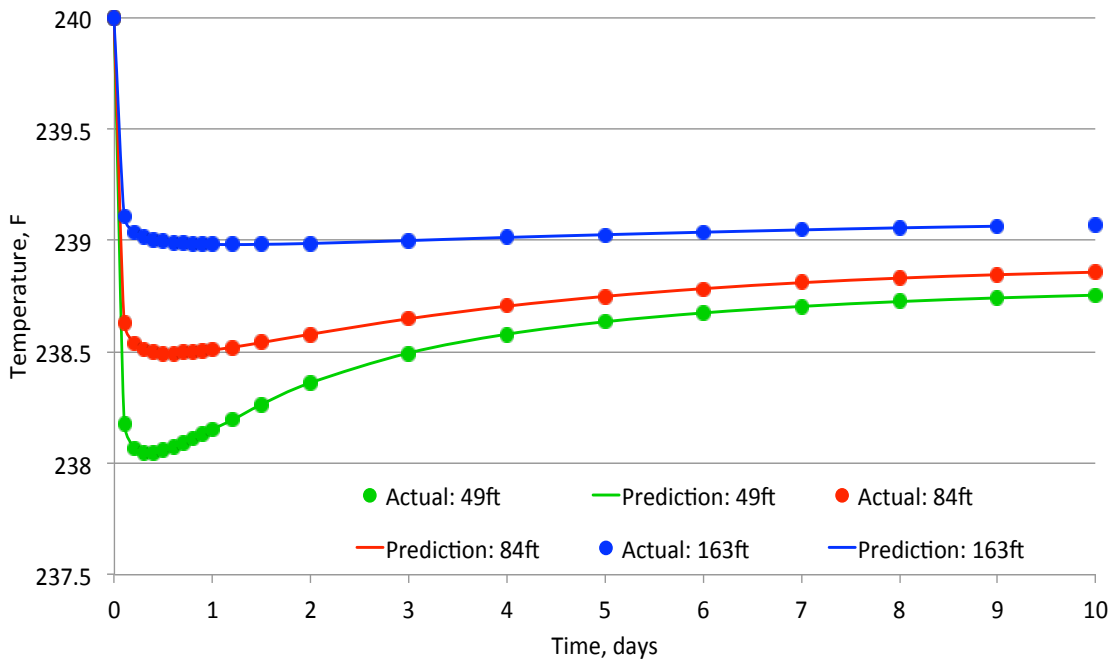

Figure 5.2: Plot showing the match results in temperature profile for the constant-thickness reservoir

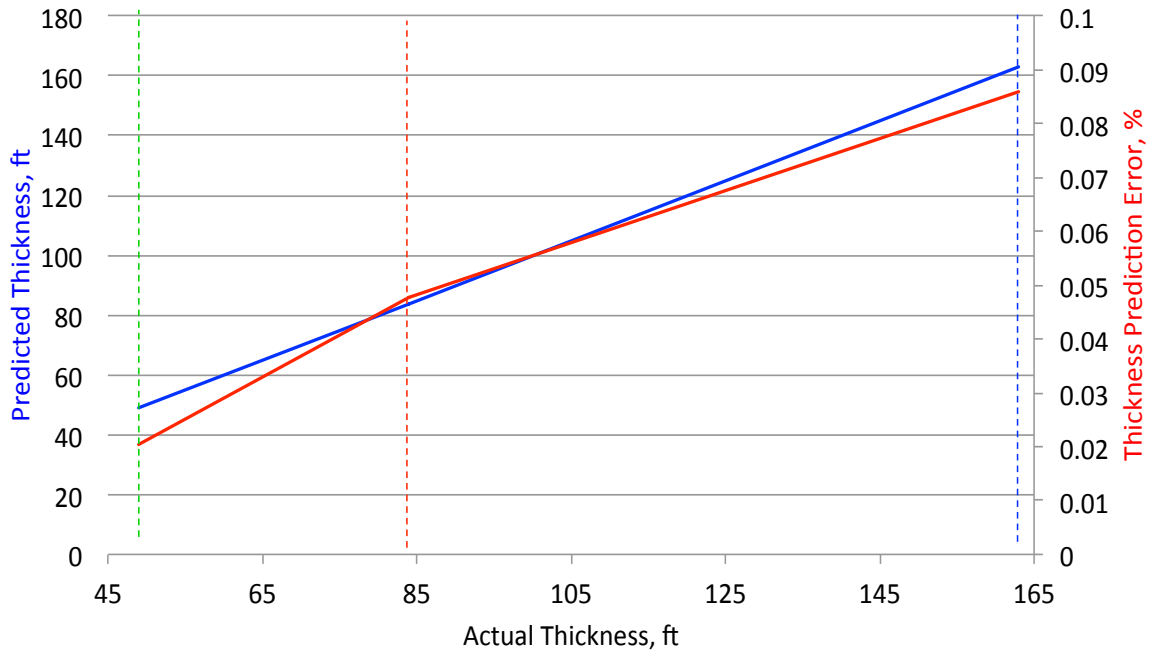

Figure 5.3: Plot showing the reservoir thickness predicted and its deviation (error) from the thickness of the actual reservoir for each of the three reservoir thickness values studied

5.2 Homogeneous Reservoir with Constant Thickness and Geothermal Gradient

The reservoir-well construction for this model is the same as that in Section 5.1 (Figure 5.1), with a geothermal gradient as depicted in Figure 5.4. Similar to the constant-thickness model with a constant initial temperature, a constant-thickness model with a geothermal gradient, Figure 5.5 gave a very good match to the actual reservoir reservoir flowing temperature. Reservoir thickness prediction, Figure 5.6

was also really good, also with a prediction error of less than 0.1%. This means that given that all other reservoir and fluid properties are known, including the geothermal gradient itself, reservoir thickness can be determined in a partially penetrating, constant-thickness reservoir.

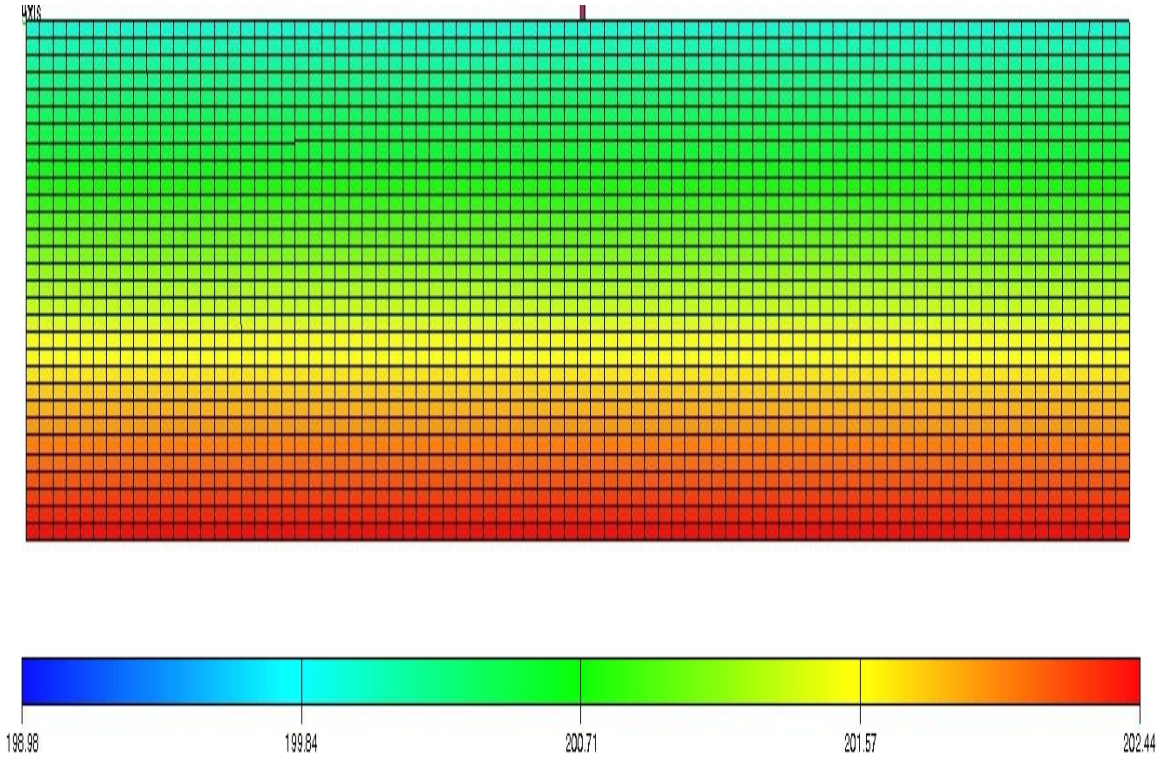

Figure 5.4: Grid showing the temperature increase with depth to simulate geothermal gradient

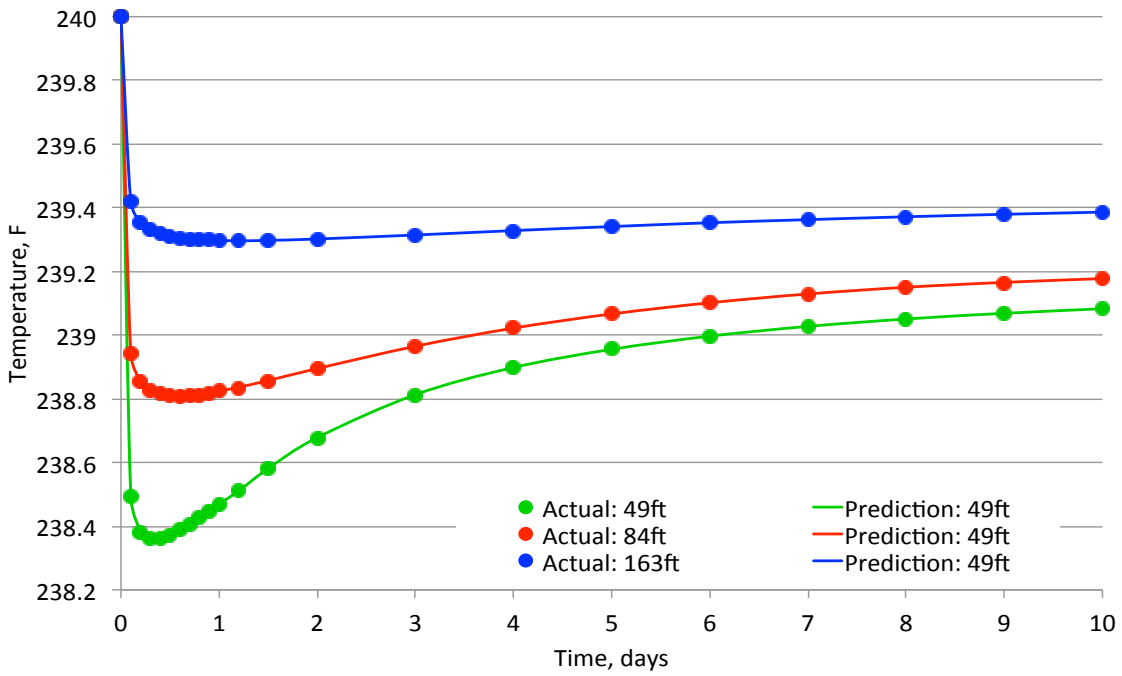

Figure 5.5: Plot showing the match results in temperature profile for the constant-thickness reservoir with a geothermal constant

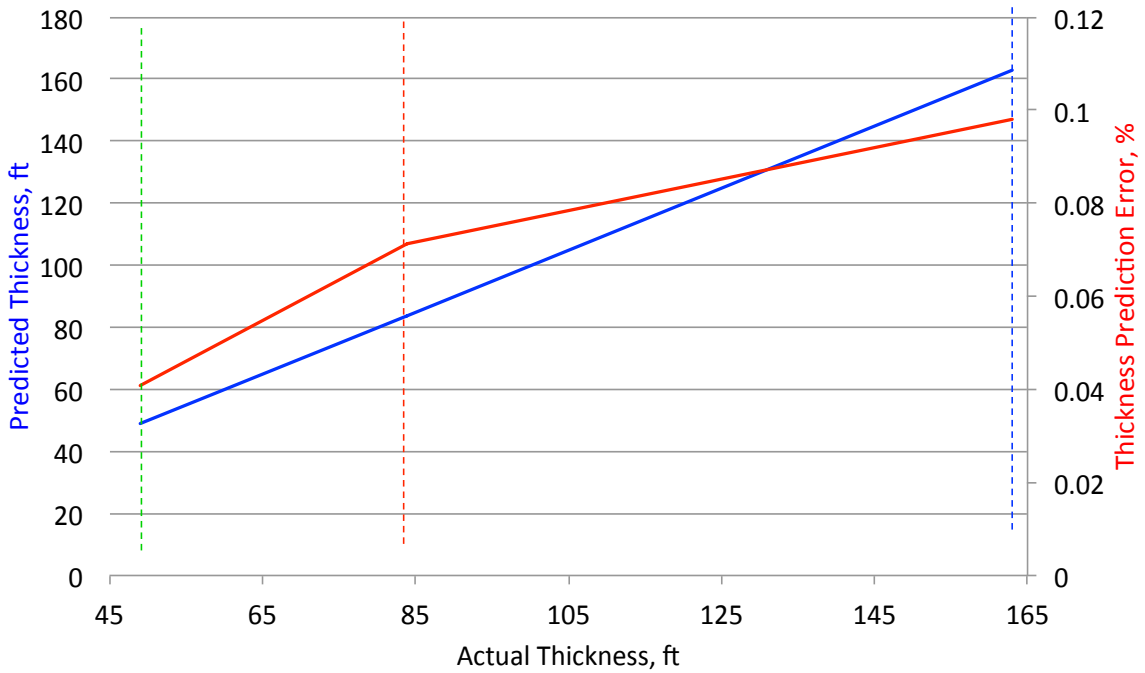

Figure 5.6: Plot showing the reservoir thickness predicted and its deviation (error) from the thickness of the actual reservoir for each of the three reservoir thickness values studied for the constant-thickness model with a geothermal gradient

5.3 Homogeneous Reservoir with Tapering Thickness and Constant Initial Reservoir Temperature

Figure 5.7 shows a schematic representing the tapered grid well fully penetrating the reservoir used for this study. The reservoir flowing temperature profile from the model varies greatly from that of the actual reservoir's in the tapered-thickness

case both model and actual reservoir temperature profiles shown in Figure 5.8. It is, therefore, no surprise that the reservoir thickness prediction error is great for all three reservoir thicknesses studied, as shown in Figure 5.9. When attempting to determine the thickness using the model, the matching model used was assumed to be of constant thickness so as to eliminate any prior assumptions about the shape of the reservoir. This, however, did not yield a good match and the thickness prediction error is high at 10% for the 49ft reservoir, 60% for the 84ft reservoir and 80% for the 163ft reservoir. The larger the reservoir thickness, the greater the reservoir prediction error. It can, therefore, be said that using a constant-thickness reservoir and not obtaining a good match gives incorrect estimates of reservoir thickness prediction but could be used as an indicator that the reservoir thickness is not constant.

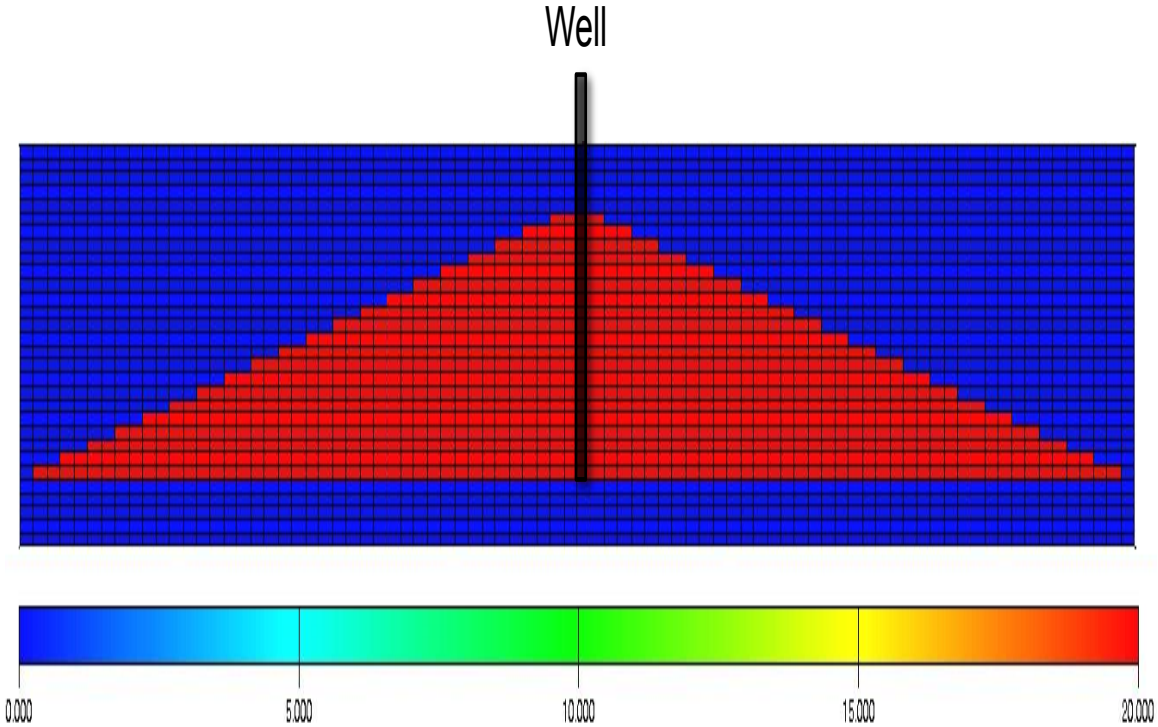

Figure 5.7: Grid for the tapered reservoir model with a well fully penetrating the thickest interval in the reservoir

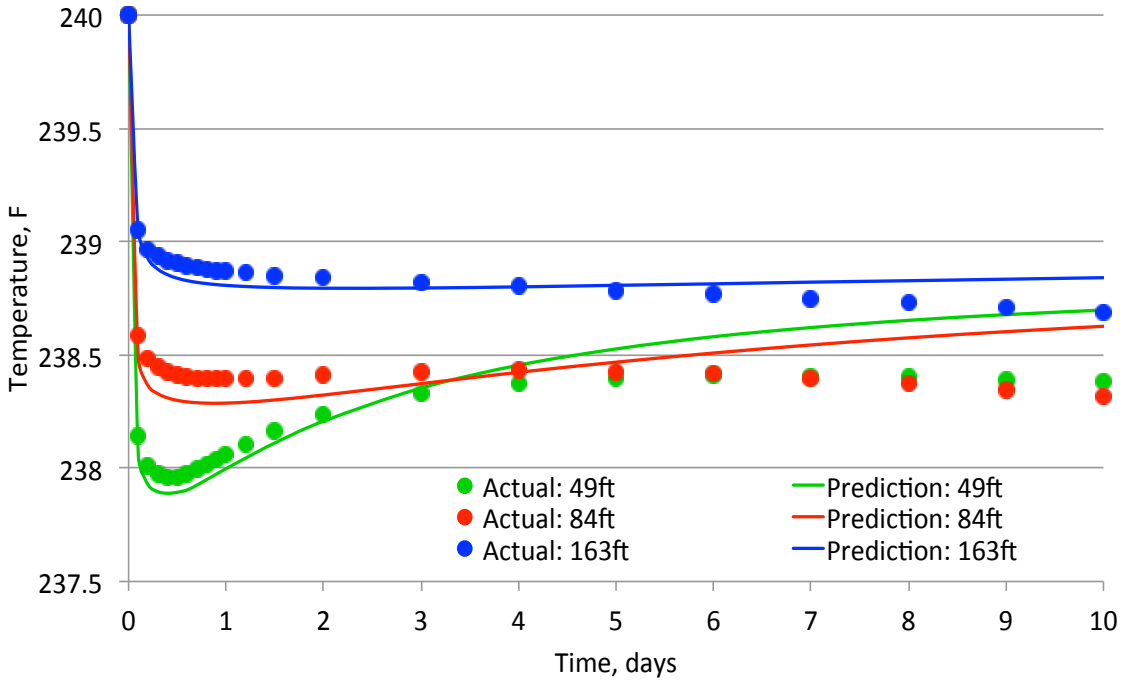

Figure 5.8: Plot showing the match results in temperature profile for the tapered-thickness reservoir

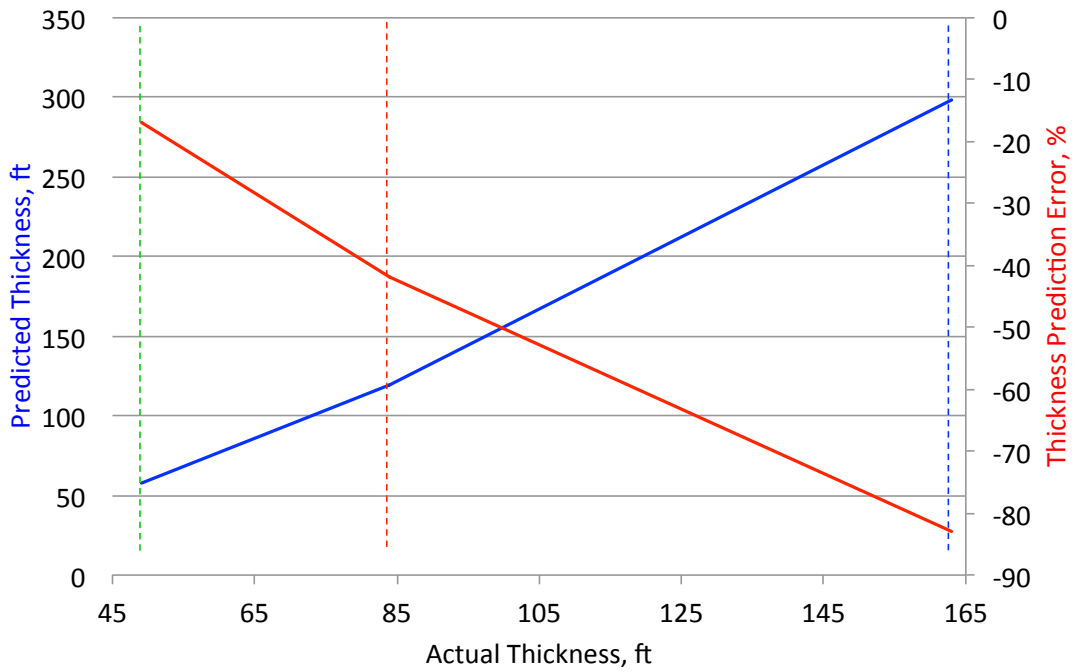

Figure 5.9: Plot showing the reservoir thickness predicted and its deviation (error) from the thickness of the actual reservoir for each of the three reservoir thickness values studied for a tapered-thickness model

5.4 Homogeneous Reservoir with Divergent Thickness and Constant Initial Reservoir Temperature

The reservoir-well arrangement representing the divergent model analysis is shown in Figure 5.10. Similar to the tapered-thickness model in Section 5.3, the matching model was assumed to be constant as no prior knowledge of the reservoir shape was

assumed. In the divergent-thickness model, we were unable to match the flowing temperature of the actual reservoir. The reservoir thickness prediction error shown in Figure 5.12 is greater than 60% for all three reservoir thicknesses investigated. Although the temperature profiles did not match the actual reservoir temperature profile, information about the nonuniformity of the reservoir can be extracted.

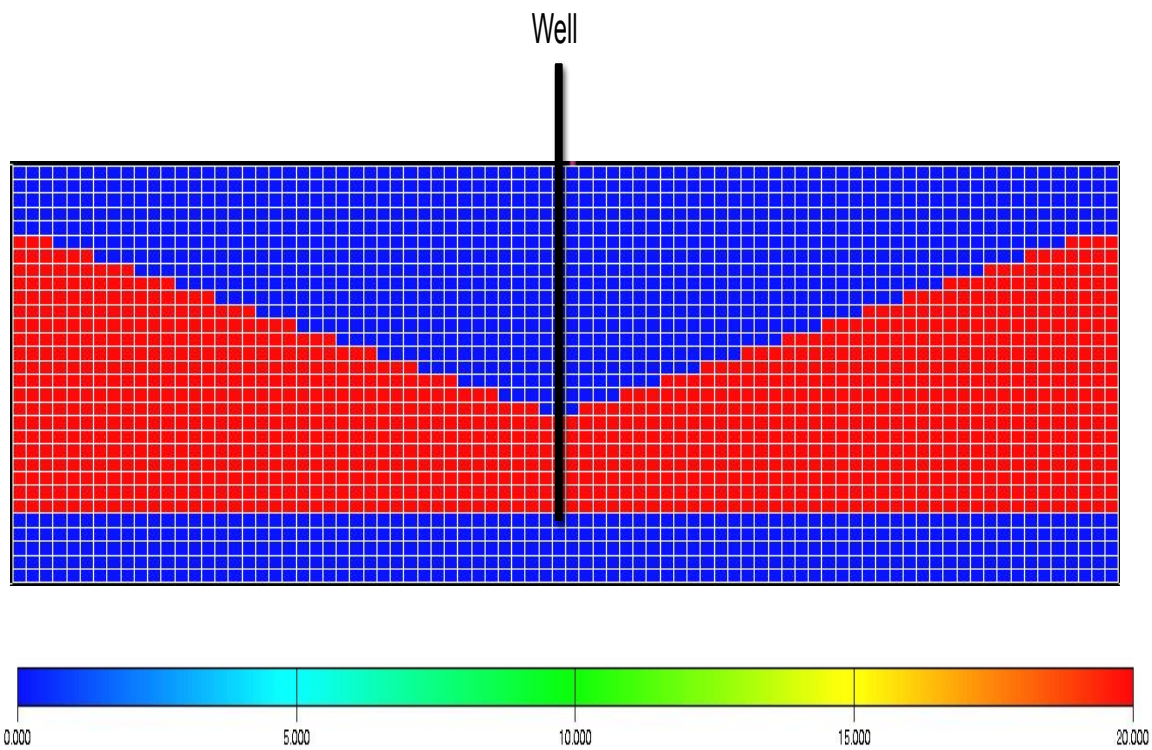

Figure 5.10: Grid for the divergent reservoir model with a well fully penetrating the thinnest interval in the reservoir

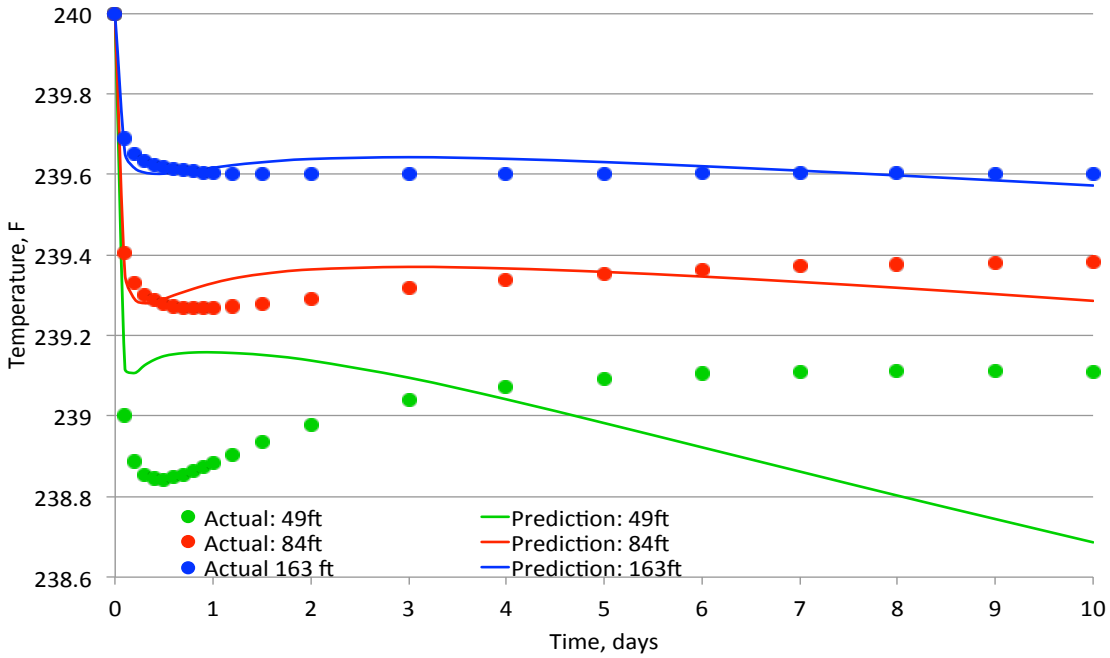

Figure 5.11: Plot showing the match results in temperature profile for the divergent-thickness reservoir

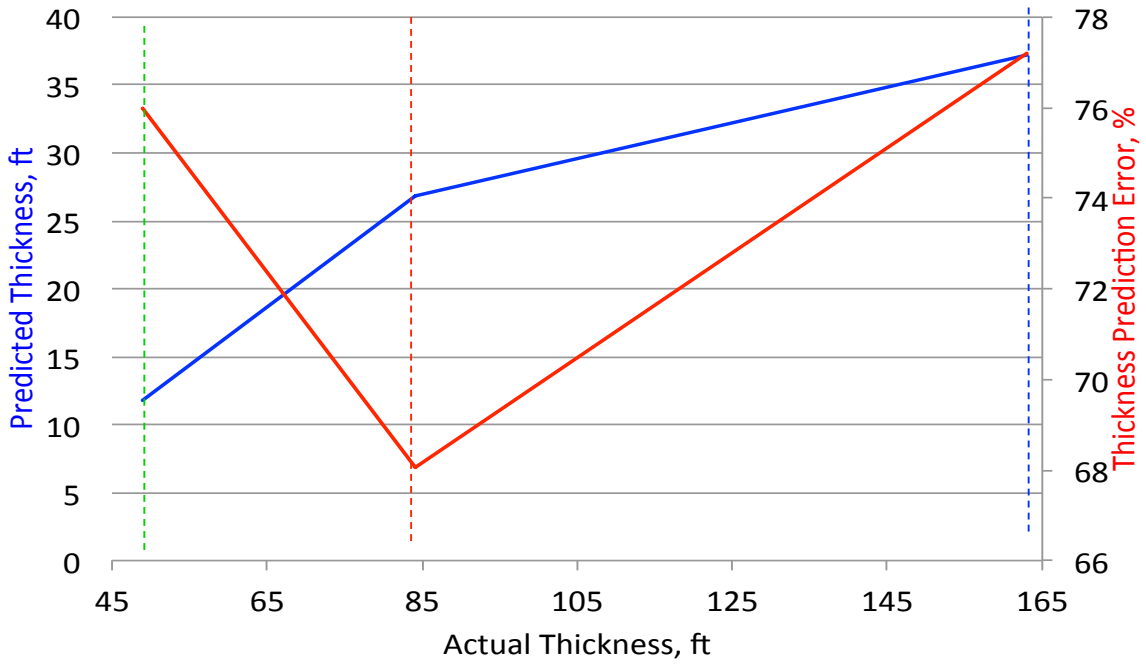

Figure 5.12: Plot showing the reservoir thickness predicted and its deviation (error) from the thickness of the actual reservoir for each of the three reservoir thickness values studied for the tapered-thickness model

5.5 Results Summary

We have shown that temperature data can be used to determine reservoir thickness in a partially-penetrated reservoir. For a reservoir whose thickness decreases away from the well or increasing away from the well (nonconstant-thickness reservoir), reservoir temperature alone is unable to provide exact information on reservoir thickness. However, we are able to extrapolate the nonuniformity of the reservoir due to the mismatch in actual reservoir and model data when using a constant-thickness

reservoir to match a nonuniform reservoir.

Chapter 6

Conclusions and Future Work

Temperature profiles used to determine reservoir thickness are most sensitive to formation porosity, rock conductivity and oil viscosity. With the knowledge of these parameters (porosity, rock conductivity and viscosity) and other fluid and formation properties, the reservoir thickness of a constant-thickness reservoir with a partially penetrating well can be determined from flowing temperature rate. When the geometry of the reservoir deviated from a constant-thickness model as in the tapered-thickness and the divergent thickness models, reservoir thickness could not be determined using temperature. However, a temperature history mismatch could be used to diagnose that the reservoir thickness is perhaps not uniform.

Temperature has shown itself to be a useful property in reservoir property analysis. It is, therefore, only fitting that work concerning the usage of temperature continue to be investigated. For this project specifically, an investigation into integrating other available information such as geologic knowledge on the shape of the reservoir to determine the thickness for a nonuniform reservoir should be undertaken. Equation 4.1 shows that the reservoir temperature is a function of more parameters that could

be investigated in a continuing sensitivity study to establish their required precision for a range of thickness prediction errors. A sensitivity study on the effects of varying fluid viscosity and density simultaneously to determine their combined effects on the use of temperature in determination of reservoir thickness could also be studied.

Geothermal thermal gradient is a naturally occurring phenomena which cannot be avoided. With all other properties of the reservoir known, a 5% offset in geothermal gradient should not deter reservoir thickness determination using temperature. However, much of our time was allocated to understanding the basic model starting with a constant-initial-temperature reservoir model. Effects of changes in geothermal gradient to reservoir thickness prediction need to be investigated further to fully understand what limitations this method would encounter in the presence of geothermal gradient.

Equation B.8 in Appendix B shows that temperature is a function of some dimensionless coefficients which if plotted, could result in a quick diagnostic method for the thickness (or shape) of the reservoir.

Once the basic model is understood, analysis of multiphase systems could lead a way towards investigating wider applicability of this idea.

Nomenclature

β	Thermal expansion coefficient
ϵ	Joule-Thomson coefficient
ϕ	Formation of porosity
ρ_f	Fluid density
ρ_s	Formation density
C_p	Specific heat of fluid at constant pressure
C_s	Specific heat of solid
K_f	Thermal conductivity of the fluid
K_s	Thermal conductivity of solid
P	Pressure
$q_f^{'''}$	Heat production
Q_cond	Net heat flow at the base/caprock
r	Radius

r_e	External radius
r_w	Wellbore radius
T	Temperature
t	Time
T_o	Temperature at time zero
V	Rate tensor

References

[1] V. Khare and A. Martinez, "Estimation of sub-tuned reservoir thickness from amplitudes at different seismic bandwidths- a time-domain approach," *Exxon-Mobil Upstream Research Company, SEG Las Vegas Annual Meeting*, 2008.

[2] M. C. Kelly and C. Skidmore, "Prediction of bed geometry net and gross reservoir thickness," *Emerald Geoscience Research, SEG International Exposition and 72nd Annual Meeting*, October 2012.

[3] D. P. Marion, D. L. Jizba, and S. Vernassa, "Porosity and reservoir thickness from core, log and seismic measurements," *SPE*, September 1994.

[4] Z. A. R. Aswad, "A simplified graphical method for estimating oil reservoir thickness," *SPE*, June 1985.

[5] C. S. Kabir and J. A. Joseph, "In search of thickness-independed permeability from transient pressure-rate data," *SPE*, September 1998.

[6] H. Elshawhawi, "Use of temperature data in gas well tests," *SPE*, October 1999.

[7] A. S. Ramazanov and A. Parshin, "Temperature distribution in oil- and water-saturated reservoir with account of oil degassing," *Oil and Gas Business*, 2006.

[8] J. Siavoshi, "A new method for reservoir characterization using temperature transients tests," *World Petroleum Council*, 2005.

[9] A. H. W.Sui, D. Zhu and C. Ehlig-Economides, "Determining multilayer formation properties from transient temperature and pressure measurements," *SPE*, 2008.

[10] O. O. Duru, "Reservoir analysis and parameter estimation constrained to temperature, pressure and flowrate histories," *Stanford*, 2011.

[11] Z. Zhang, "Joint inversion of production and temperature data for the identification of permeability distribution with depth in deep reservoirs," *SPE*, 2013.

[12] E. C. Robertson, "Thermal properties of rocks," *USGS*, 1988.

[13] P. Bandyopadhyay, "Robust nonlinear regression methods for parameter estimation in pressure transient analysis, chapter 2," June 2014.

[14] A. Ramazanov and V. Nagimov, "Analytical model for the calculation of temperature distribution in the oil reservoir during unsteady fluid inflow," *Oil and Gas Business*, September 2007.

[15] D. Nield and A. Bejan, "Convection in porous media, chapter 2," June.

Appendix A

Sample Input File

```
RUNSPEC ==================
TITLE – title of the run Temperature dependence on reservoir thickness/
DIMENS
—Nx Ny Nz‘ 82 82 30/
OIL WATER FIELD DEADOIL
THERMAL
START —Start date for simulation
1 ’JAN’ 2013/
WELLDIMS
1/
GRID ==================
—THCONR —201720*25/
THCROCK 201720*50/
THCOIL 201720*3/
THCWATER 201720*0.6/
```

HEATCR 201720*35 /

TOPS 6724*5000 /

DXV 82*20/

DYV 82*20/

DZV

30*10/

PERMX 33620*0 134480*20 33620*0 /

PERMY 33620*0 134480*20 33620*0 /

PERMZ 33620*0 134480*20 33620*0 /

PORO

33620*0.001 134480*.23 33620*0.001 /

PROPS ==========

VISCREF 2750/

PVTW – Pref — wat FVF @Pref — wat compres — visco@Pref — viscosibility @Pref 14.7 1.0 5.0E-7 1.0 0.0 /

– PRESSURE RS BO VISO CO VISOSIBILITY – [psia] [mscf/stb] [rb/stb] [cp] [1/psia] [1/psia] PVCO 14 0 1 .6 1.E-05 0.0 2750 0 .8 .6 1.E-05 0.0 /

OILCOMPR 5E-7 0.000178 0/

ZFACT1 0.1/

OILSPECH 0.15/

ROCK – reference Pressure and rock compressibility 14.7 1E-6 /

DENSITY – oil wat gas @surface(lbm/scf) 40.0 62.238 /

OILVISCT 180 3 200 3 /

– SWAT KRW PCOW SWFN

– Sw Krw Pcow —— —— —- 0.27 0.0 24 0.4397 0.0476 6 0.51 0.0952 3 0.56 0.1428 2 0.62 0.1905 1.5 0.65 0.2381 1.2 0.68 0.2857 0.0 0.7151 0.3333 0.0 1 0.50 0.0// – FOR

OIL-WATER AND OIL-GAS-CONNATE WATER CASES – – SOIL KROW SOF3 – So Krow Krog —— —— —— 0.27 0 0 0.4397 .1 .1 0.51 .2857 .2857 0.56 .3 .3 0.62 .4 .4 0.65 .6 .6 0.68 .8 .8 0.7151 .99 .99 1 1 1 /

SGFN 0 0 0 .04 0 .2 .1 .022 .5 .2 .1 1 .6 .5 3 .88 1 3.9 /

SOLUTION == initial state of solution variables ======= SOIL 201720*1 /

SWAT 201720*0 /

PRESSURE 201720*3500 /

TEMPI 201720*240 /

SUMMARY == output written to summary *.RSM file ====== RUNSUM – additional table in *.PRT file WOPR – 'W'ell 'O'il 'P'roduction 'R'ate 'PROD'

WWPR – 'W'ell 'W'ater 'P'roduction 'R'ate 'PROD'

WBHP – and the bottom hole pressure of 'PROD' 'PROD'

FPR – Average reservoir pressure FOPT – Cumulative oil production of the field, ('F'ield 'O'il 'P'roduction 'T'otal)

WTEMP —WELL TEMPERATURE 'PROD'

BTEMP – request temperature output for specified blocks for each time step 42 42 6 /

/

SCHEDULE == operations to be simulated ======

RPTONLY

RPTRST – request restart file 'BASIC=2' /

TUNING – min/max timestep (3 sections) 0.1 50 / 5* 0.1 / 2* 100 /

WELSPECS == WELL SPECIFICATION DATA ======== – WELL GROUP LOCATION BHP PI – NAME NAME I J DEPTH DEFN 'PROD' 'W1' 42 42 -1 'OIL' 2* 'STOP' / – see ECL Manual for details / COMPDAT – COMPLETION SPECIFICATION DATA – WELL LOCATION OPEN/ SAT CONN WELL KH S

D AXIS – NAME I J K1 K2 SHUT TAB FACT DIAM 'PROD' 42 42 6 10 'OPEN' 0 -1 0.5 / –see ECL manual for details / WCONPROD – PRODUCTION WELL CONTROLS – WELL OPEN/ CTRL OIL WATER GAS LIQU RES BHP – NAME SHUT MODE RATE RATE RATE RATE RATE 'PROD' 'OPEN' 'ORAT' 1000 4* 50 / –see ECL manual for details /

– timesteps can be refined by entering multiple TSTEP keywords TIME – and run it for 10 days 0.1 0.2 0.3 0.4 0.5 0.6 0.7 0.8 0.9 1 1.2 1.5 2 3 4 5 6 7 8 9 10/

END ==========

Appendix B

Analytical Solution

From Bejan and Nield [15], the energy balance equation is given by:

$$[(1-\phi)(\rho C_p)_f]\frac{\delta T}{\delta t} + (\rho C_p)_f.\mathbf{v}.\nabla.T = \nabla.\{[(1-\phi)k_s + \phi k_f]\nabla T\} + Q_{cond} + q_f^{'''} \quad \text{(B.1)}$$

where,

C_p=Specific heat of fluid at constant P

C_s=Specific heat of solid

k_s=Thermal conductivity of solid

k_f=Thermal conductivity of fluid

ρ=density

ϕ=porosity

q'''=heat production

Q_cond=Net heat flow at base/caprock

$$q_f^{'''} = \beta T \phi C_f \frac{\delta P}{\delta t} - \epsilon V \nabla P \tag{B.2}$$

where,

β=thermal expansion coefficient

ϵ=Joule-Thomson coeffient

If we let:

$C_T = [((1-\phi)(\rho_C)_s + \phi(\rho C_p)_f,$

and

$k_T = [(1-\phi)(\rho C)_s + \phi(\rho C_p)_f]$

Equation B.1 becomes:

$$C_T \frac{\delta T}{\delta t} + (\rho C_p)_f . \mathbf{v} . \frac{\delta T}{\delta r} = k_T \frac{1}{r} \frac{\delta}{\delta r} r \frac{\delta T}{\delta r}] + \beta T \phi \frac{\delta P}{\delta t} - \epsilon V \frac{\delta P}{\delta r} \tag{B.3}$$

Let:

$C = \frac{(\rho C_p)_f}{C_T}$

$K = \frac{k_T}{C_T}$

$\theta = \frac{\beta T \phi}{C_T}$

$E = \frac{\epsilon}{C_T}$

$$\frac{\delta T}{\delta t} + (CV - \frac{K}{r}\frac{\delta T}{\delta t} - \theta\frac{\delta P}{\delta t} + EV\frac{\delta P}{\delta r} = 0 \tag{B.4}$$

The following temperature solution derivation is based on the work by Ramazanov and Nagimov [14]. Assuming conductivity is negligible,

$$T(r_w, t) = T_o + \frac{E}{C}[P(r_w, 0) - P(r_w, t)] - (\frac{E}{C} + \theta)\int_0^t \frac{\delta P}{\delta t}dt \tag{B.5}$$

where,

T_o= intial reservoir temperature

The general pressure solution is given by

$$P(r, t) = P_i + \frac{P_i - P(r_w, t)}{lnR} ln\frac{r}{r_e} \tag{B.6}$$

where

$R = \frac{r_w}{r_e}$

and,

r_w = wellbore radius

r_e= external reservoir radius

Using an average time τ, and the pressure solution equation, Equation B.6, Equation B.5 becomes:

$$T(r_w,t) = T_o + \frac{E}{C}[P(r_w,0) - P(r_w,t)] - (\frac{E}{C} + \theta)[P_i - P(r_w,t) + P(r_w,\tau) - P(r_x,\tau) \tag{B.7}$$

where,

$r_x = r_w^2 + 2a + [P_i\tau - S(\tau]$

$a = -\frac{CK}{\mu ln(R)}$

$S(\tau) = int_0^\tau P(\tau)d\tau$

Finally, Ramazanov and Nagimov arrived at:

$$\begin{aligned} T(r_w,t) = T_o + \frac{\epsilon}{(\rho C_p)_f}[P(r_w,0) - P(r_w,t)] - (\frac{\epsilon}{(\rho C_p)_f} \\ + \frac{\beta T\phi}{(1-\phi)(\rho C)_s + \phi((\rho C_p)_f})[P_i - P(r_w,t) + P(r_w,\tau) - P(r_x,\tau) \end{aligned} \tag{B.8}$$

Appendix C

Additional Plots for Sensitivity Analyses

C.1 Sensitivity to Porosity

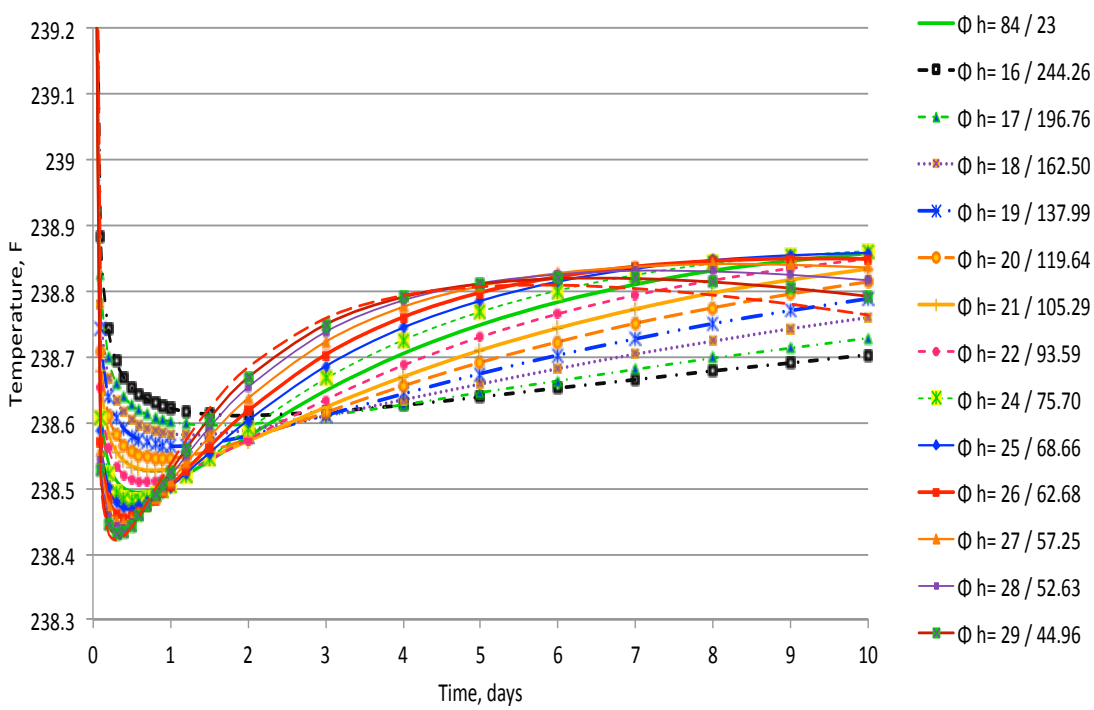

Figure C.1: Plot showing the best match results in temperature profile with the uncertainty in reservoir porosity for 84ft reservoir where h is the thickness predicted for the porosity shown

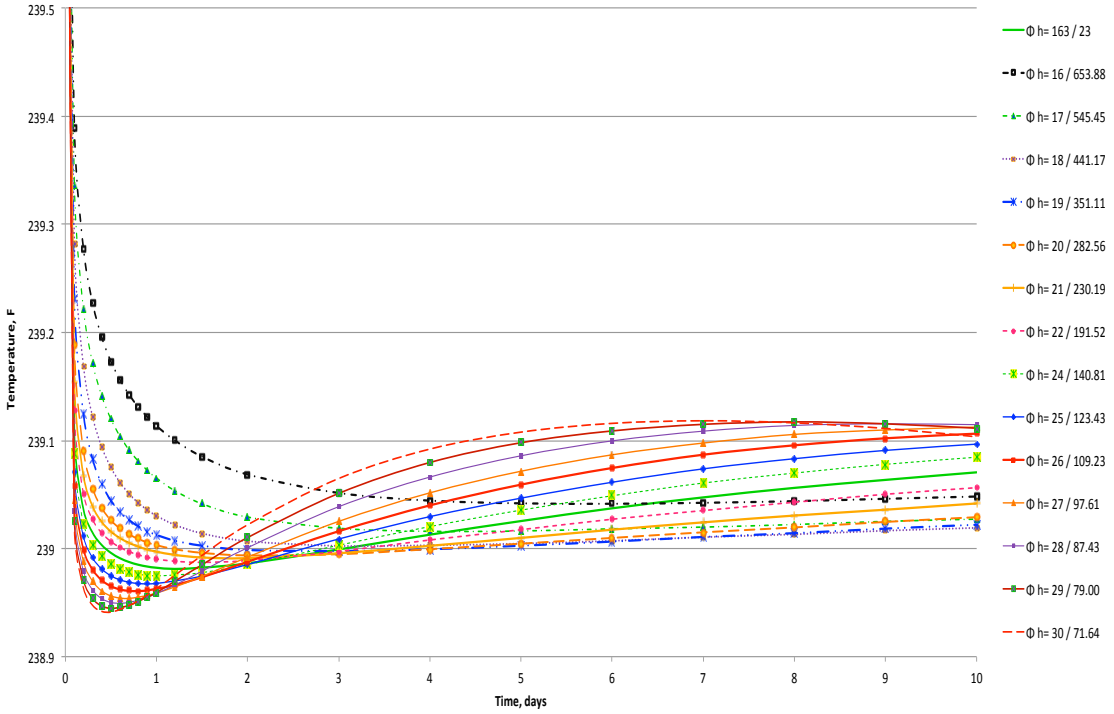

Figure C.2: Plot showing the best match results in temperature profile with the uncertainty in reservoir porosity for 163ft reservoir where h is the thickness predicted for the porosity shown

C.2 Sensitivity to Formation Heat Conductivity

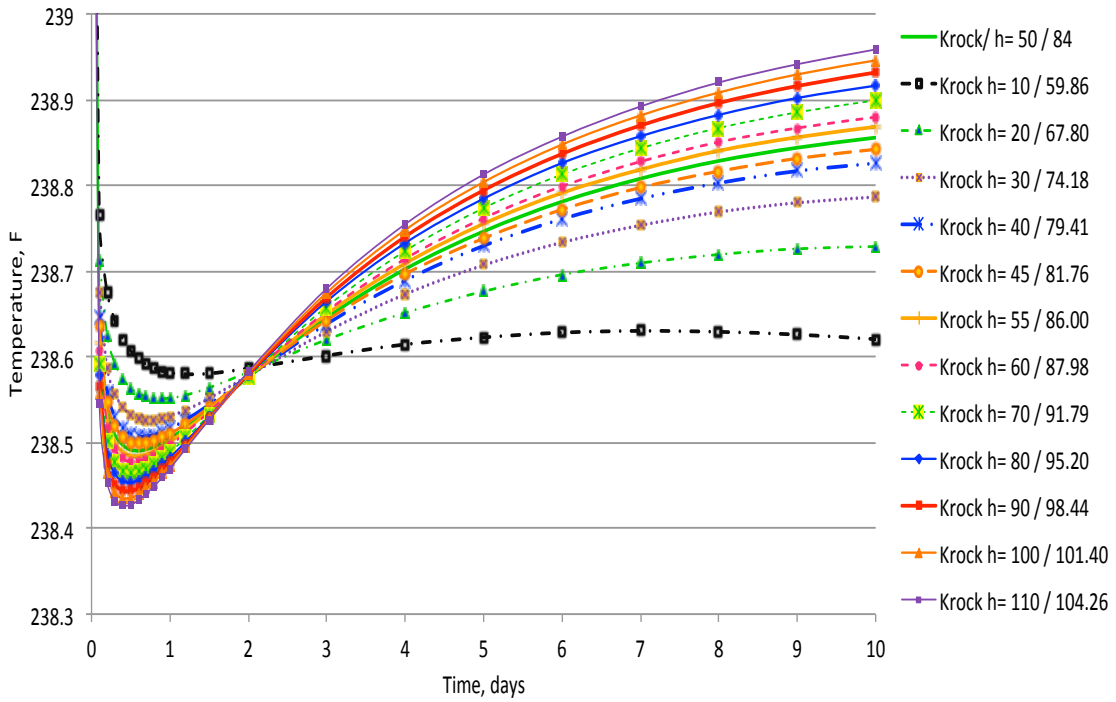

Figure C.3: Plot showing the best match results in temperature profile with the uncertainty in reservoir conductivity for 84ft reservoir where h is the thickness predicted for the heat conductivity shown

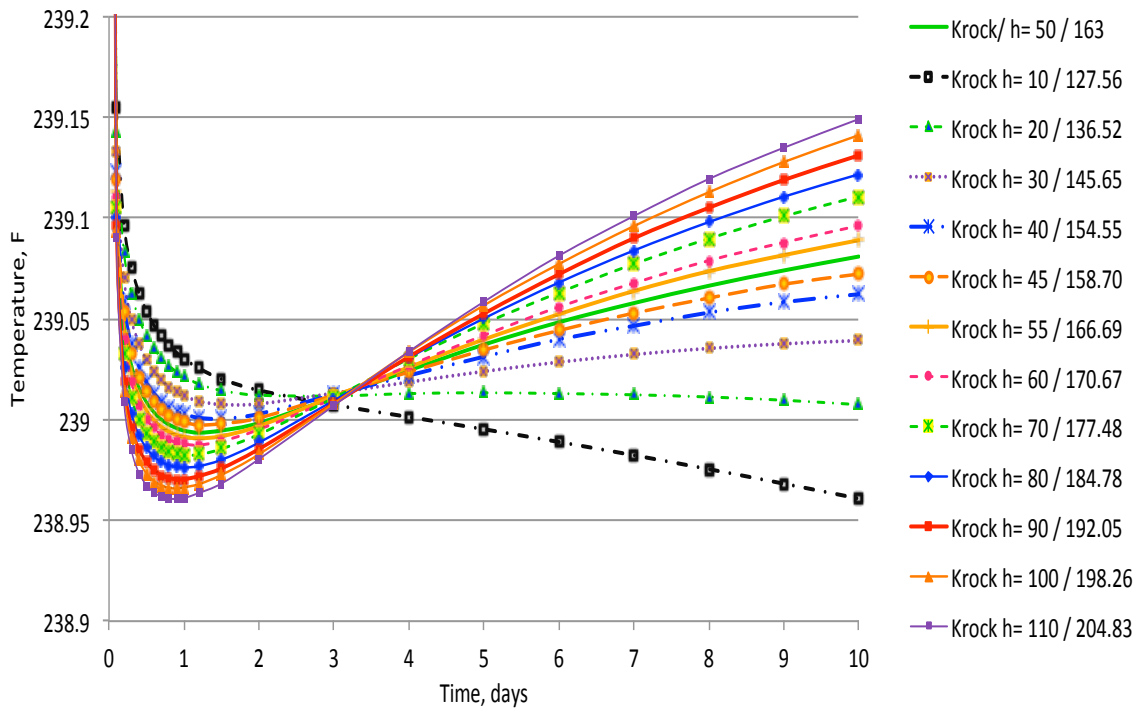

Figure C.4: Plot showing the best match results in temperature profile with the uncertainty in reservoir conductivity for 163ft reservoir where h is the thickness predicted for the heat conductivity shown

C.3 Sensitivity to Oil Density

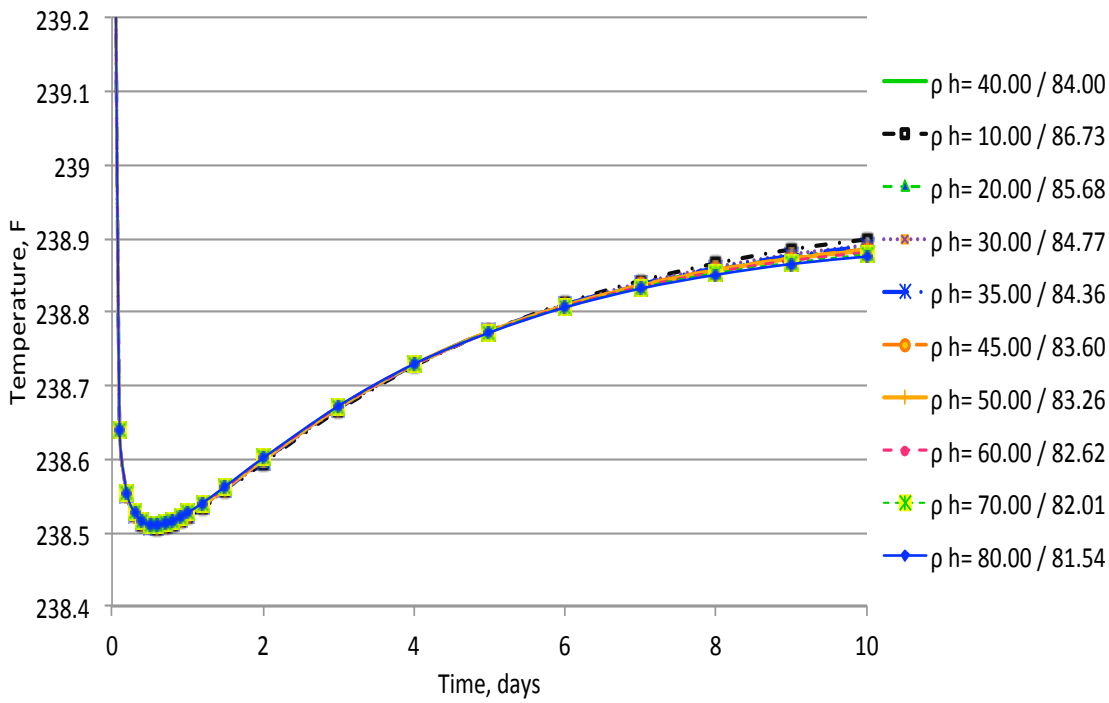

Figure C.5: Plot showing the best match results in temperature profile with the uncertainty in oil density for 84ft reservoir where h is the thickness predicted for the oil density shown

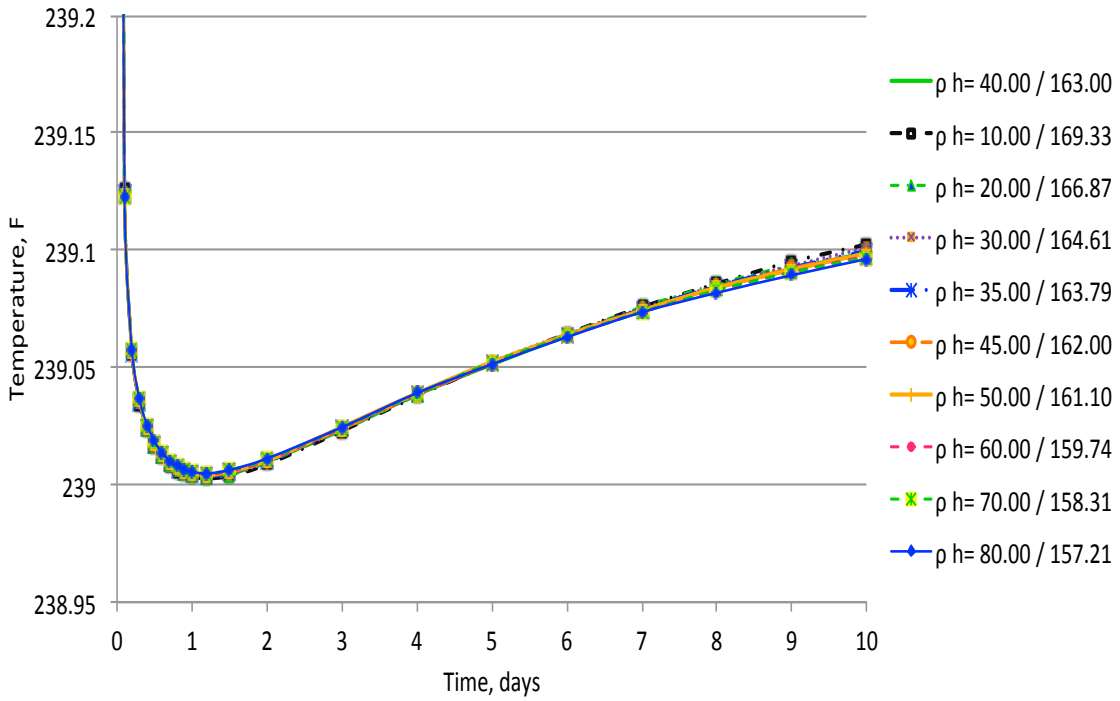

Figure C.6: Plot showing the best match results in temperature profile with the uncertainty in oil density for 163ft reservoir where h is the thickness predicted for the oil density shown

C.4 Sensitivity to Specific Heat

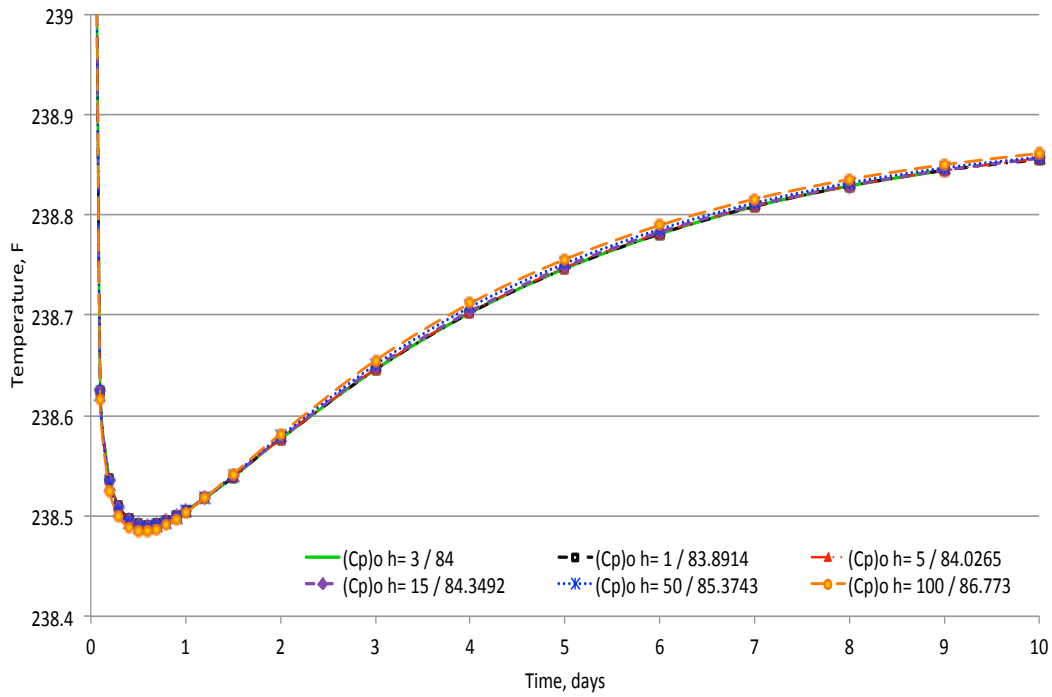

Figure C.7: Plot showing the best match results in temperature profile with the uncertainty in oil specific heat for 84ft reservoir where h is the thickness predicted for the specific heat shown

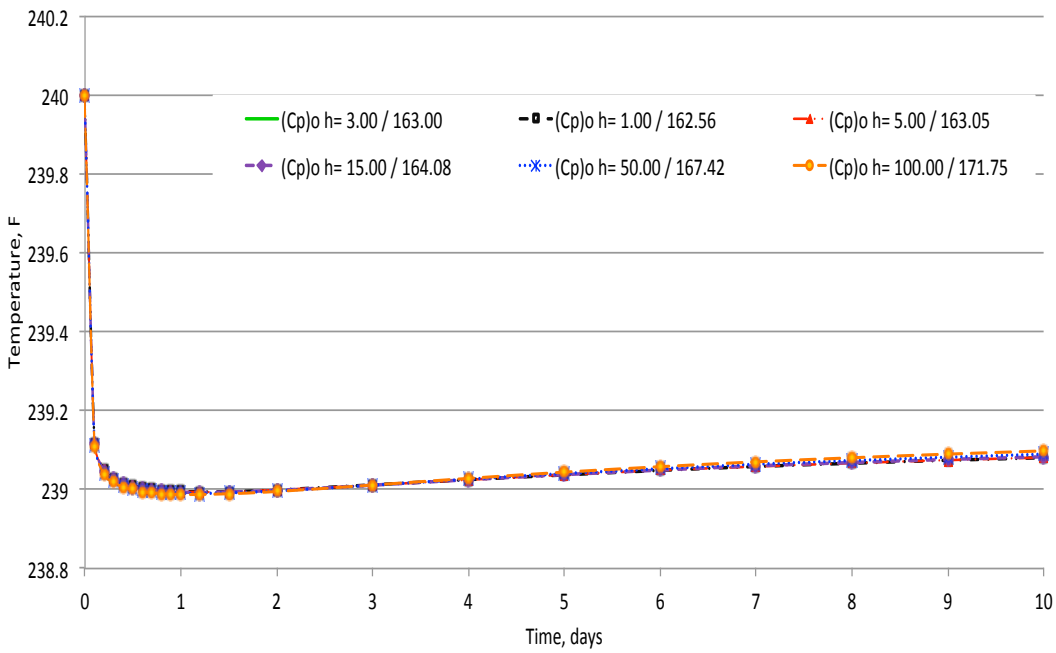

Figure C.8: Plot showing the best match results in temperature profile with the uncertainty in oil specific heat for 163ft reservoir where h is the thickness predicted for the specific heat shown

C.5 Sensitivity to Thermal Expansion Coefficient

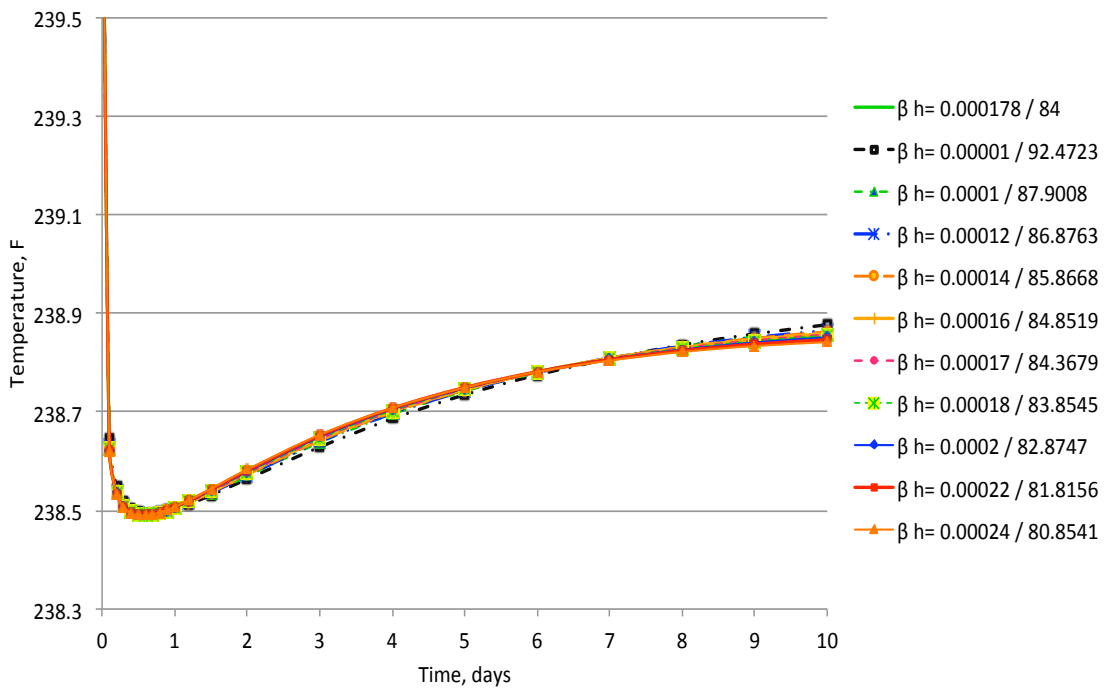

Figure C.9: Plot showing the best match results in temperature profile with the uncertainty in thermal expansion coefficient for the 84ft thick reservoir where h is the thickness predicted for the thermal expansion coefficient shown

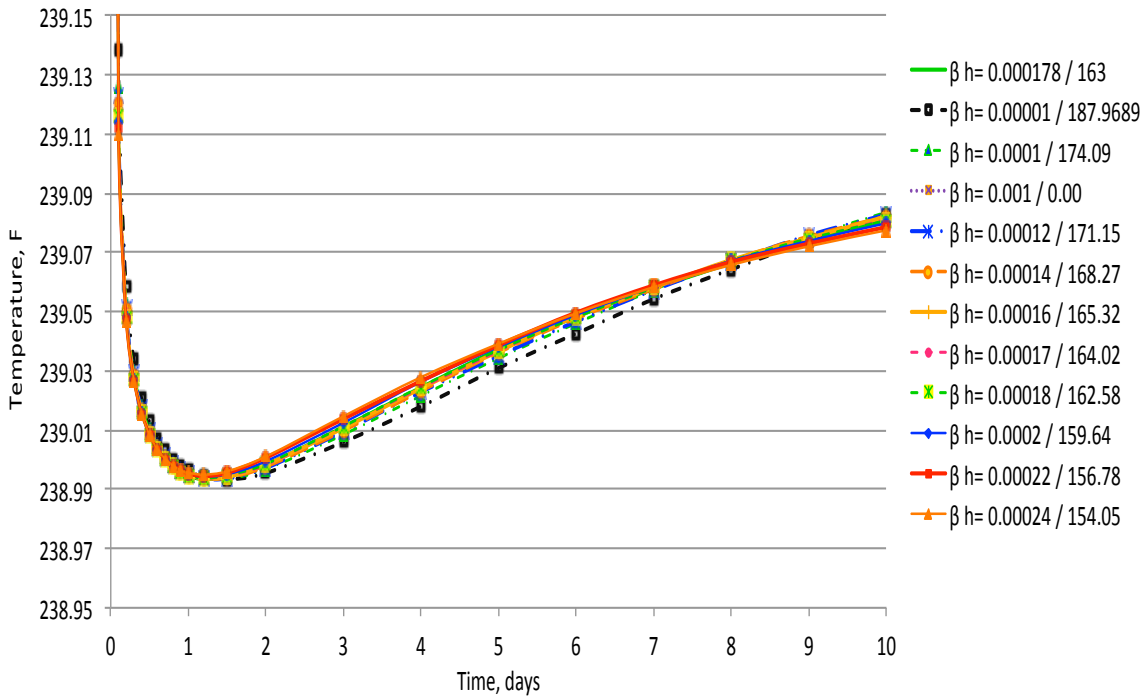

Figure C.10: Plot showing the best match results in temperature profile with the uncertainty in thermal expansion coefficient for the 163ft thick reservoir where h is the thickness predicted for the thermal expansion coefficient shown

C.6 Sensitivity to Oil Viscosity

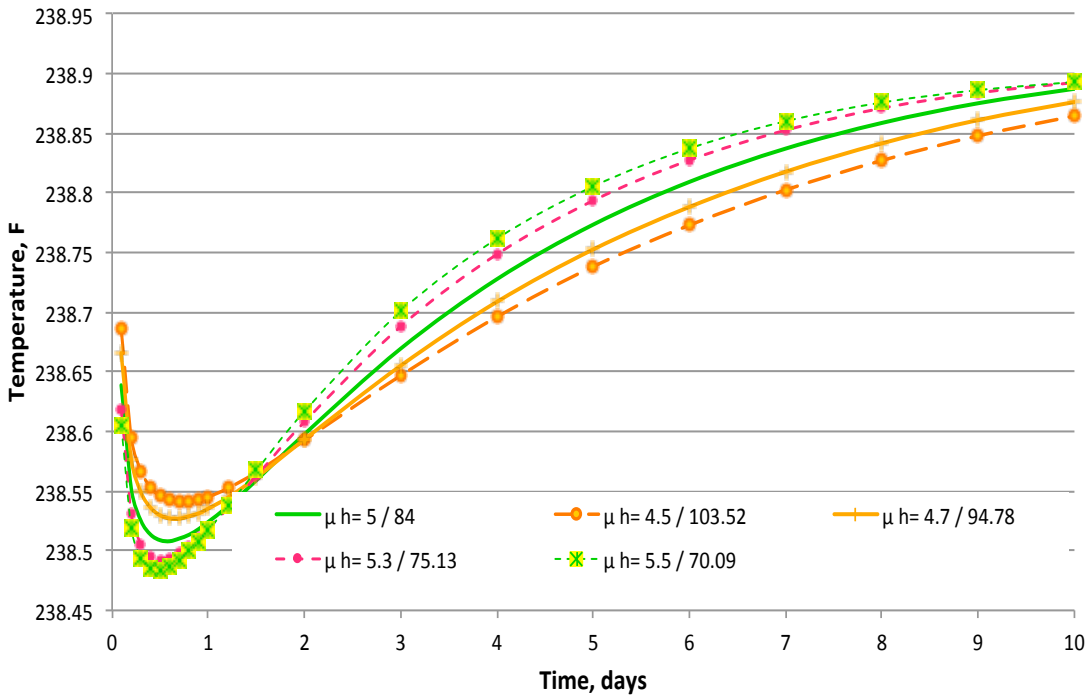

Figure C.11: Plot showing the best match results in temperature profile with the uncertainty in oil viscosity for the 84ft thick reservoir where h is the thickness predicted for the oil viscosity shown

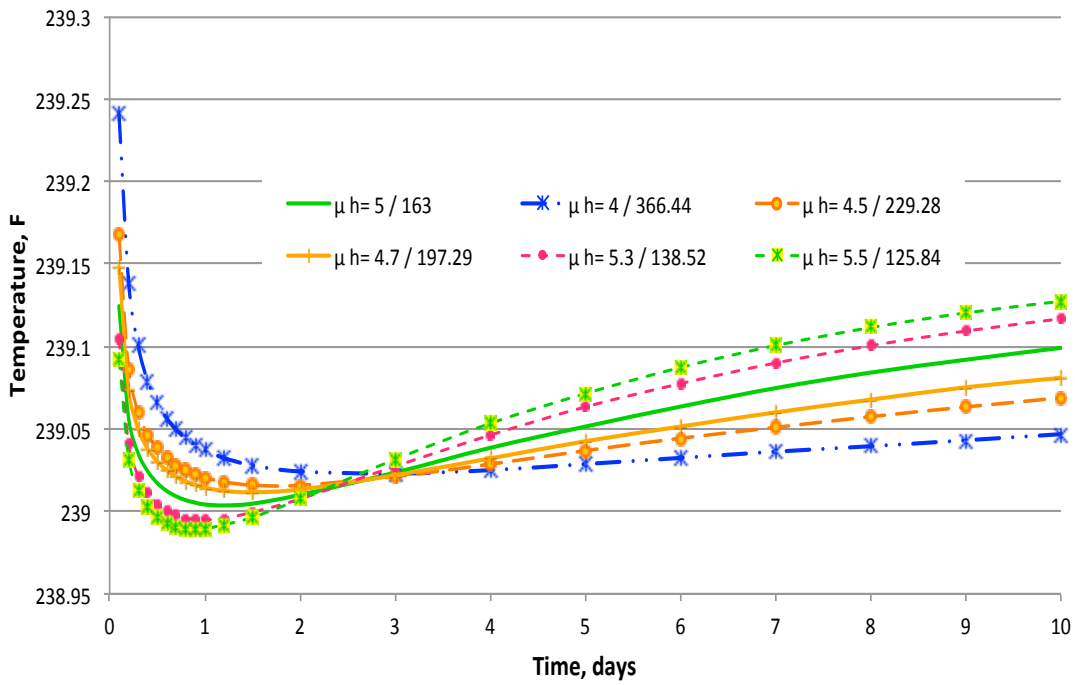

Figure C.12: Plot showing the best match results in temperature profile with the uncertainty in oil viscosity for the 163ft thick reservoir where h is the thickness predicted for the oil viscosity shown